Article

Antibiotic combinations reduce *Staphylococcus aureus* clearance

https://doi.org/10.1038/s41586-022-05260-5

Received: 17 December 2020

Accepted: 22 August 2022

Published online: 5 October 2022

Check for updates

Viktória Lázár[1,5,6], Olga Snitser[1], Daniel Barkan[2] & Roy Kishony[1,3,4]✉

The spread of antibiotic resistance is attracting increased attention to combination-based treatments. Although drug combinations have been studied extensively for their effects on bacterial growth[1–11], much less is known about their effects on bacterial long-term clearance, especially at cidal, clinically relevant concentrations[12–14]. Here, using en masse microplating and automated image analysis, we systematically quantify *Staphylococcus aureus* survival during prolonged exposure to pairwise and higher-order cidal drug combinations. By quantifying growth inhibition, early killing and longer-term population clearance by all pairs of 14 antibiotics, we find that clearance interactions are qualitatively different, often showing reciprocal suppression whereby the efficacy of the drug mixture is weaker than any of the individual drugs alone. Furthermore, in contrast to growth inhibition[6–10] and early killing, clearance efficacy decreases rather than increases as more drugs are added. However, specific drugs targeting non-growing persisters[15–17] circumvent these suppressive effects. Competition experiments show that reciprocal suppressive drug combinations select against resistance to any of the individual drugs, even counteracting methicillin-resistant *Staphylococcus aureus* both in vitro and in a *Galleria mellonella* larva model. As a consequence, adding a β-lactamase inhibitor that is commonly used to potentiate treatment against β-lactam-resistant strains can reduce rather than increase treatment efficacy. Together, these results underscore the importance of systematic mapping the long-term clearance efficacy of drug combinations for designing more-effective, resistance-proof multidrug regimes.

Antibiotics are the most effective tool to treat bacterial infections, but bacteria are rapidly developing both resistance and persistence to these drugs[18,19]. The use of antibiotics has increased steadily over the past 15 years and is now further increasing due to the ongoing coronavirus pandemic; nearly all patients with severe COVID-19 are receiving antibiotics to prevent and treat secondary bacterial infections[20]. Meanwhile, bacterial pathogens—most prominently, the widespread opportunistic pathogen *Staphylococcus aureus*—are evolving ways to evade antibiotic killing through various mechanisms of resistance[21,22] as well as persistence[23,24], whereby a small isogenic subpopulation of bacteria undergoes a phenotypic change to temporarily avoid the cidal effect of the antibiotic[25]. Antibiotic persistence leads to a biphasic killing curve, beginning with an early phase of rapid killing of the normal cells and continuing with a later phase of a much slower killing of the persistent cells[26]. Persistence can therefore reduce the ultimate infection clearance efficacy of antibiotic treatments[27].

As pathogens evolve resistance and persistence to antibiotics, drug combinations are gaining increased attention[28]. Multidrug therapies can have potential benefits in increasing the spectrum of targeted pathogens, preventing the emergence of antibiotic resistance and improving clinical efficacy[29–33]. Considering the effects of subinhibitory drug combination on bacterial growth (growth–inhibition interactions), laboratory studies have found that the potency of drug mixes increases with the number of co-mixed drugs, yet specific drug pairs and multidrug combinations can substantially deviate from this general trend due to drug synergy and antagonism[1–11]. Considering the bactericidal effects of drug combination, drug antagonism is commonly revealed, especially between static and cidal drugs[2,3,34–40]. In some cases, drug antagonism can be so strong that the combined effect of co-mixed drugs is weaker not only compared with their expected additive effects but also compared with the effect of one of the drugs alone[12,31–33,41]. Such suppressive, or hyperantagonistic, interactions are typically non-reciprocal—the combined effect of the drugs is weaker than one of the mixed components but not the other (one drug suppresses the effect of the other, but not vice versa)[2,12,33,41]. In principle, drug combinations of which the effect is weaker than the effects of either one of the individual drug components are also possible (reciprocal suppression). However, despite the potential clinical implications of such reciprocal suppression—which, while jeopardizing drug efficacy, may counteract resistance[12,31–33]—such extreme interactions are not observed in drug combination effects on bacterial growth inhibition or on the early-killing phase.

[1]Faculty of Biology, Technion–Israel Institute of Technology, Haifa, Israel. [2]Koret School of Veterinary Medicine, The Robert H. Smith Faculty of Agricultural, Food & Environment, The Hebrew University of Jerusalem, Jerusalem, Israel. [3]Faculty of Computer Science, Technion–Israel Institute of Technology, Haifa, Israel. [4]Faculty of Biomedical Engineering, Technion–Israel Institute of Technology, Haifa, Israel. [5]Present address: HCEMM-BRC Pharmacodinamic Drug Interaction Research Group, Szeged, Hungary. [6]Present address: Synthetic and Systems Biology Unit, Institute of Biochemistry, Biological Research Centre, Szeged, Hungary. ✉e-mail: rkishony@technion.ac.il

Although drug combination effects on growth inhibition have been systematically mapped[1–11], much less is known about how drugs combine to affect longer-term population clearance and persistence (clearance interactions)[12–14]. Measuring bacterial survival after prolonged exposures to individual drugs and drug combinations is inherently difficult as it requires the quantification of low densities of surviving cells, and the use of conventional plating techniques limit the number of antimicrobial combinations that can be tested[42]. Initial studies mapping the effect of specific drug pairs on intermediate (2–4 h) or long-term clearance (8 h) identified synergistic, antagonistic as well as non-reciprocal suppressive interactions[12–14]. At longer-term survival (1 day exposure), there is even an example of reciprocal suppression[43]. Owing to the lack of a high-throughput approach to quantify cell viability en masse, a systematic study of such clearance interactions is lacking. It is therefore unclear to what extent these clearance interactions correlate with early-killing and growth-inhibition interactions, how the overall clearance efficacy varies with the number of co-mixed drugs, and whether reciprocal suppression could be identified and used to counteract resistance to the single drugs.

High-throughput cell-viability assay

To systematically quantify bacterial survival under a range of drug combinations, we adapted a high-throughput cell-viability assay based on miniaturized plating and automated image analysis[44]. In brief, growing *S. aureus* bacterial cultures were treated with individual drugs or drug mixes. Then, at several time points after drug exposure, the cultures were microplated at a range of dilutions. Automated imaging and image analysis enabled the quantification of the number of microcolonies grown at each microplating spot (up to 100 colonies were detected in each microplating spot in a 96-well format) (Methods and Fig. 1a). Detection sensitivity and reliable colony counting was facilitated by differential labelling and co-culturing of the same *S. aureus* strain with two different fluorescent markers (DsRed and GFP). Using this assay, we comprehensively quantified the effect of pairwise and multidrug mixes on the early- and late-killing phases of a drug-sensitive *S. aureus* strain as well as on the competition among drug-sensitive and drug-resistant strains (Methods; a total of over 25,000 microplating images).

Drug interactions in early killing

Mapping the growth inhibition and early-killing interactions among all pairwise combinations within a set of 14 diverse antibiotics (Supplementary Table 1) revealed two distinct networks of synergistic, antagonistic and non-reciprocal suppressive interactions (Extended Data Fig. 1). Inspired by previous studies[7,12], we defined for each pair of drugs A and B two-directional interaction scores signifying the effect of drug A on drug B and the effect of drug B on drug A. For early killing, directional interactions were defined on the basis of measurements of the decrease in cell viability during 90 min after exposure to each of the 14 drugs when applied individually (each drug A is applied at a fixed cidal concentration $A_{1\times}$ chosen on the plateau of its dose–response curve, and at double this concentration, $A_{2\times} = 2 \times A_{1\times}$; Extended Data Fig. 2a and Supplementary Table 1) and when applied in pairwise combinations ($A_{1\times} + B_{1\times}$) (Methods and Fig. 1b). For growth inhibition, directional interactions were defined based on measurements of the 90% inhibition isobole in two-dimensional concentration gradients of each drug pair (Methods and Extended Data Figs. 1a–d and 3). Both the early-killing and growth-inhibition networks showed interactions ranging from synergistic to antagonistic and non-reciprocal suppression, yet these interactions were not correlated among the two networks (Extended Data Fig. 2b) (for example, protein-synthesis inhibitors suppress the efficacy of trimethoprim on the growth inhibition but not on the killing efficacy) (Extended Data Figs. 1e,f and 3–5). Non-reciprocal suppression was more common in killing interactions, mirroring the classical suppression of the killing activity of cidal drugs by static protein synthesis drugs[2,3,38,45,46] (even though these 'classically static' drugs are in fact bactericidal against *S. aureus* at concentrations used clinically and as used in our study[47–49]). Although non-reciprocal suppression was common, reciprocal suppression was not detected in the inhibitory or the early-killing networks (Extended Data Figs. 1e,f, 3 and 4).

Drug interactions in long-term clearance

In contrast to early-killing and growth-inhibition interactions, quantifying the effects of antibiotic combinations on long-term clearance revealed pronounced and widespread reciprocal suppression, especially among combinations of cell-wall and classically static protein-synthesis inhibitors (Fig. 1c). To quantify clearance interactions, we measured cell viability during 8 h exposure to cidal concentrations of individual drugs and drug pair combinations and calculated their directional interaction scores (as defined above) (Fig. 1b and Methods). These clearance interactions were not correlated with the growth inhibition interactions but were strongly correlated with the early-killing interactions, indicating that the long-term effect of the drug combinations can be predicted, to some extent, from the early-killing efficacy (Extended Data Fig. 2c,d). However, we also discovered some substantial differences between the early-killing and late-clearance interactions. Indeed, some strong non-reciprocal suppressive early-killing interactions, such as the suppression of the early-killing activity of the cidal drugs by the classically static drugs, are weakened or completely diminished at longer time scales (such as the effect of protein-synthesis inhibitors on the early-killing efficacy of tobramycin and the effect of the trimethoprim on the early-killing efficacy of cell-wall inhibitors or ciprofloxacin) (Fig. 1c and Extended Data Figs. 1f, 4 and 5). By contrast, many other known early-killing non-reciprocal suppressive interactions were strongly enhanced at longer time scales, often developing into reciprocal suppression. In particular, we found that, when cell-wall and classically static protein-synthesis inhibitors are combined, the persisting bacterial population is larger than when any of the drugs are administered alone, even at the same dose and despite using both drugs at cidal concentrations (Fig. 1c and Extended Data Fig. 5). These reciprocal suppressive clearance interactions were robust to changes in drug concentrations, growth environments, incubation time and bacterial physiological state, and were also present in an unrelated *S. aureus* strain with a different genetic background (Methods and Extended Data Fig. 6a–e). Furthermore, such suppression also appeared in human serum and in an in vivo infection model of the larva of the great wax moth (*G. mellonella*) (Methods, Fig. 1d and Extended Data Fig. 6b,d,f,g). However, note that suppression observed in the larvae is weaker, especially in the direction of protein-synthesis inhibitors suppressing β-lactams and seems dependent on the physiological stage of the larvae, as well as on drug concentrations (in particular, suppression was not observed at lower drug concentrations and in competition among strains) (Extended Data Fig. 6h,i).

Multidrug-reduced long-term clearance

Not only was reciprocal suppression common among drug pairs, increasing the number of drugs beyond two further reduced the efficacy of long-term clearance. Following the same procedure used for the drug pairs, we measured the population survival in the presence of all possible multidrug mixes of six commonly used cidal and classically static drugs (clindamycin (CLI), tetracycline (TET), fusidic acid (FUS), meropenem (MER), ciprofloxacin (CPR), oxacillin (OXA); 63 combinations) (Fig. 2a, Extended Data Fig. 7a and Supplementary Table 1). In contrast to the growth inhibitory effects of multidrug combinations, for which potency increases with the number of drugs[6–10], focusing on long-term clearance, we found the opposite behaviour—increasing the

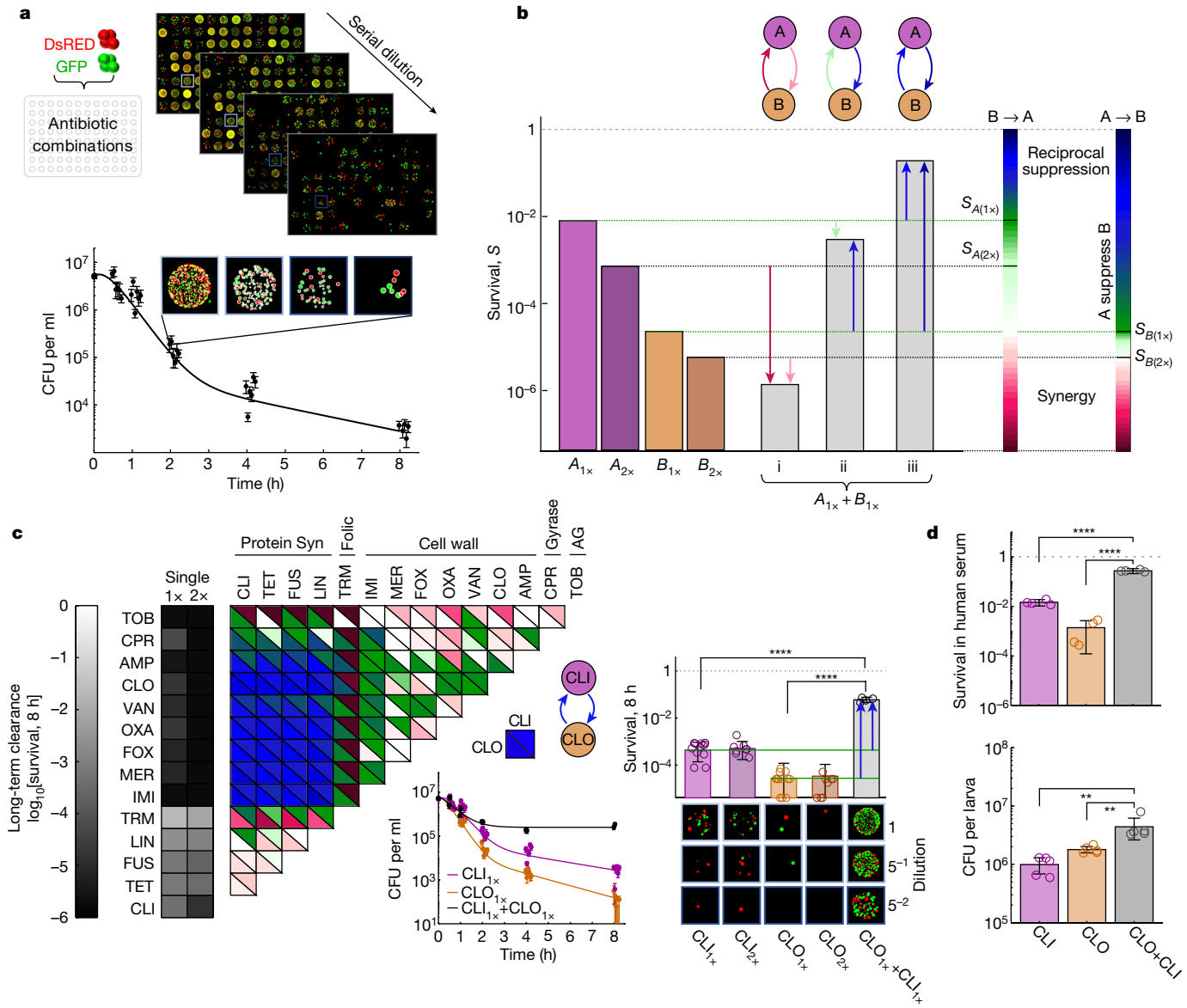

Fig. 1 | Systematic quantification of pairwise drug interactions reveals emergent reciprocal suppression in long-term population clearance. **a**, Cell viability over time after antibiotic treatment was measured by high-throughput microplating and automated image analysis of a mixed DsRed- and GFP-tagged *S. aureus* strain. Example data are shown for treatment with CLI ($n = 6$ wells; fivefold serial dilution microplate images are shown for one replicate at one time point). **b**, Schematic of directional interactions. Contrasting survival after a combined treatment with two drugs, A and B, at a fixed cidal concentration (Supplementary Table 1, grey bars, S_{A+B}); the survival under drugs A and B alone at the same or double the concentration ($S_{A(1\times)}$, $S_{A(2\times)}$ (purple bars); $S_{B(1\times)}$, $S_{B(2\times)}$ (orange bars)) defines two-directional interaction scores for the effect of drug B on drug A (B→A, left colour scale) and the effect of A on B (A→B, right colour scale). The combined effect could be synergistic ($S_{A+B} < \min[S_{A(2\times)}, S_{B(2\times)}]$) (i); non-reciprocal suppressive ($S_{B(1\times)} < S_{A+B} < S_{A(1\times)}$, A suppresses B) (ii); or reciprocal suppressive ($S_{A+B} > \max[S_{A(1\times)}, S_{B(1\times)}]$) (iii). **c**, Measurements of directional interaction scores for pairwise combinations of 14 antibiotics in long-term clearance efficacy (2 strains were measured in $A_{1\times}$, $A_{2\times}$ and $A_{1\times}+B_{1\times}$ in 6, 4 and 2 experiments, respectively). The top (bottom) triangles show the interaction score for the effect of the drugs in the row (column) on the drugs in the column (row). Inset: the killing curves and final survival fraction for a representative suppressive drug combination (CLI + CLO). Statistical analysis was performed using z-tests; $P < 10^{-10}$. Points on the axis are below the detection limit. For each treatment, representative microplating images of one replicate are shown. **d**, Bacteria viability after 8 h exposure to CLI–CLO in human serum (top; 2 strains were measured in 2 experiments; $P < 10^{-10}$, two-tailed z-tests) and in *G. mellonella* larvae (**d**, bottom; $n = 10$ AROL larvae, homogenized and plated in 5 pairs; from left to right, $P = 0.008$ and $P = 0.008$, two-tailed Mann–Whitney U-tests). For **a**, **c** and **d**, the error bars represent the 95% confidence intervals calculated from the colony counts by the Poisson's model (**a** and **c** (middle)) or 2× s.e.m. (**c** (right) and **d**).

number of drugs reduces the overall clearance efficacy of the combinations (Fig. 2a and Extended Data Fig. 7a,b). This phenomenon is unique to long-term clearance interactions; whereas long-term efficacy decreased with the number of drugs, early-killing efficacy did not change across the different multidrug combinations (Extended Data Fig. 7c). The same trend was also observed in an independent set of five additional drugs of diverse classes (cefoxitin (FOX), linezolid (LIN), cefazolin (CEF), minocycline (MIN) and pristinamycin (PRI); Fig. 2b and Extended Data Fig. 8). Furthermore, considering each multidrug set as a combination of two drug mixes (for example, mix ABC is decomposed to AB + C, A + BC, AC + B), we found enrichment of reciprocal suppressions between drug mixes (Fig. 2c and Extended Data Fig. 7d), which was not observed in early-killing interactions (Extended Data Fig. 7e). Separating drug sets by all-cidal and all-static or combined drug mixes

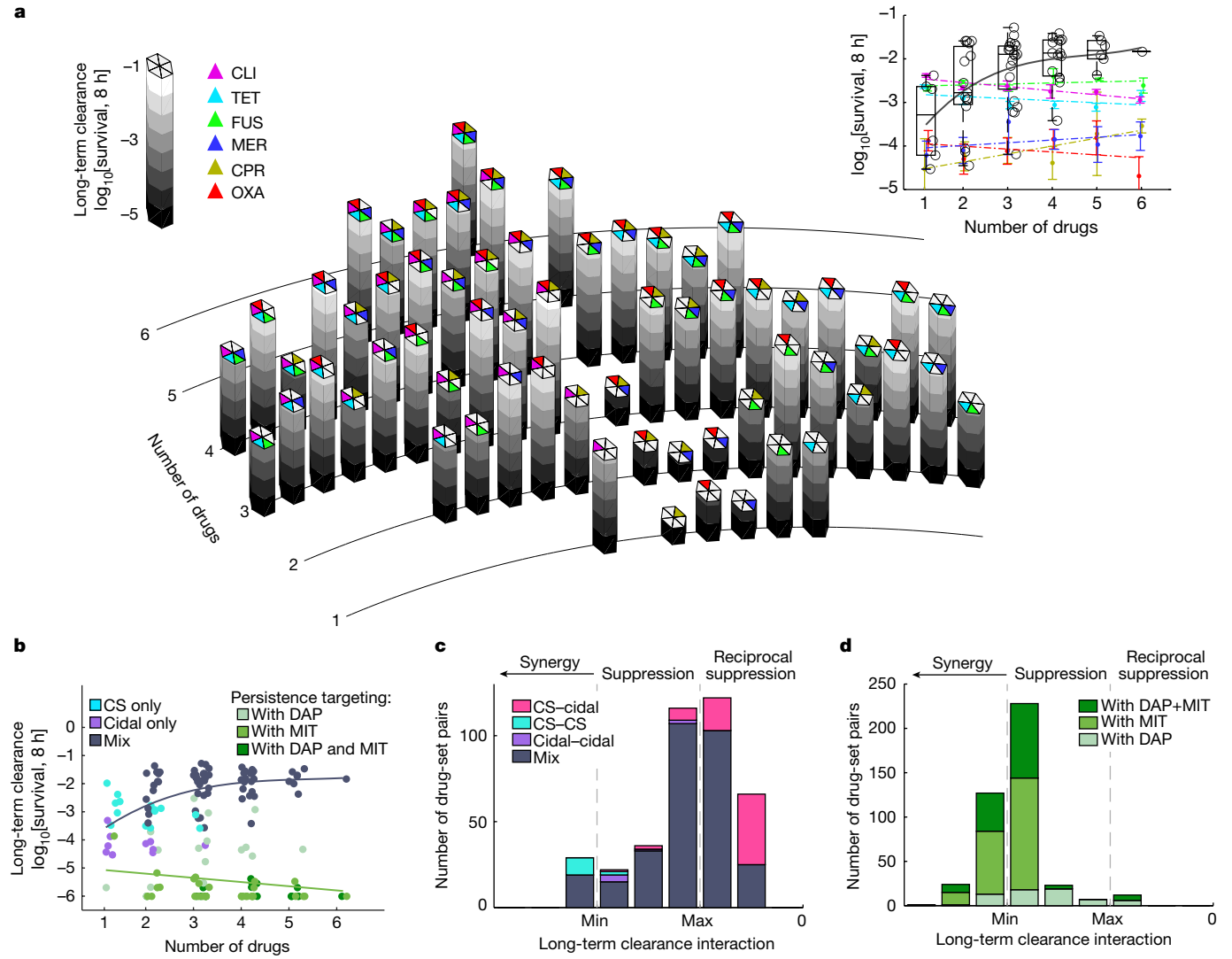

Fig. 2 | In absence of persistence-targeting drugs, long-term clearance efficacy is reduced as more drugs are added. a, Bacterial survival fraction after 8 h exposure to all possible combinations of six drugs ($2^6 = 64$), including 3 commonly used cidal (MD-cidal: MER, CPR, OXA) and 3 classically static drugs (CS: CLI, TET, FUS; Supplementary Table 1). Two strains were measured in two experiments. Inset: the survival fraction as a function of the number of co-mixed drugs (black circles; in contrast to survival fraction under each of the single drugs at increased dosage from 1× to 6× of the dosage used in the combination (coloured dots, coloured linear fits; data are mean ± 95% confidence intervals). The box plots show the median (centre line); the upper and lower quartiles (box limits); and the maximum and minimum values (whiskers); the grey line shows the quadratic fit. **b**, The survival fraction as described in the inset of **a**, but including combinations of two additional cidal (FOX, CEF) and three additional CS drugs (LIN, MIN, PRI) as well two weakly metabolic-dependent cidal drugs (MIT, DAP; persistence-targeting) (Extended Data Fig. 8). The dot colour represents drug combinations that are only CS (cyan), only cidal (purple) or a mix (grey, black cubic fit), and sets including persistence-targeting drugs (green shades; green linear fit). **c**,**d**, The distribution of the interaction scores among all tested non-overlapping pairs of drug sets (for example, drug mix ABC is decomposed into AB + C, A + BC, AC + B) without (**c**) and with (**d**) persistence-targeting drugs. $n = 391$ (**c**) and $n = 422$ (**d**). The combined effect of the drug mix is shown relative to the minimum (min) and maximum (max) of the effect of the two drug sets (Methods). Drug mix pairs are classified as only cidal (purple), only CS (cyan), mix of all CS and all cidal (pink), pairs of mixed drug sets (mix, grey) or sets including DAP or MIT (green shades).

highlights that this reciprocal suppression is mostly driven by combinations of cidal and classically static drugs (Fig. 2b,c). However, including specific drugs of which the cidal activity is only weakly dependent on cell metabolism[15–17] strongly synergized the clearance efficacy of all of the other drugs and drug mixes, efficiently eradicating the long-term surviving cell population (persistence-targeting: daptomycin (DAP), mitomycin (MIT)) (Fig. 2b,d and Extended Data Fig. 8). Our results thereby indicate that, in contrast to their combined effect on growth inhibition, multidrug mixtures commonly reduce rather than increase long-term clearance efficacy and that, although common among many drug classes, such reduced efficacy can be prevented by drugs that are effective against metabolically inactive cells.

Selection against antibiotic resistance

Next, we competed drug-resistant and drug-sensitive strains in mixtures of reciprocal suppressive drug pairs, and we found that these interactions can select against strains that are resistant to either of the single drugs. It has been shown that non-reciprocal suppressive interactions can reverse the selective advantage of a strain that is resistant to one of the drugs (if drug A suppresses drug B, the combination of the two drugs selects against resistance to drug A, but not against resistance to drug B)[12,33]. Extrapolating from these results, it has been hypothesized that, with reciprocal suppression, it might be possible to select against any of the single-drug-resistant mutants[31].

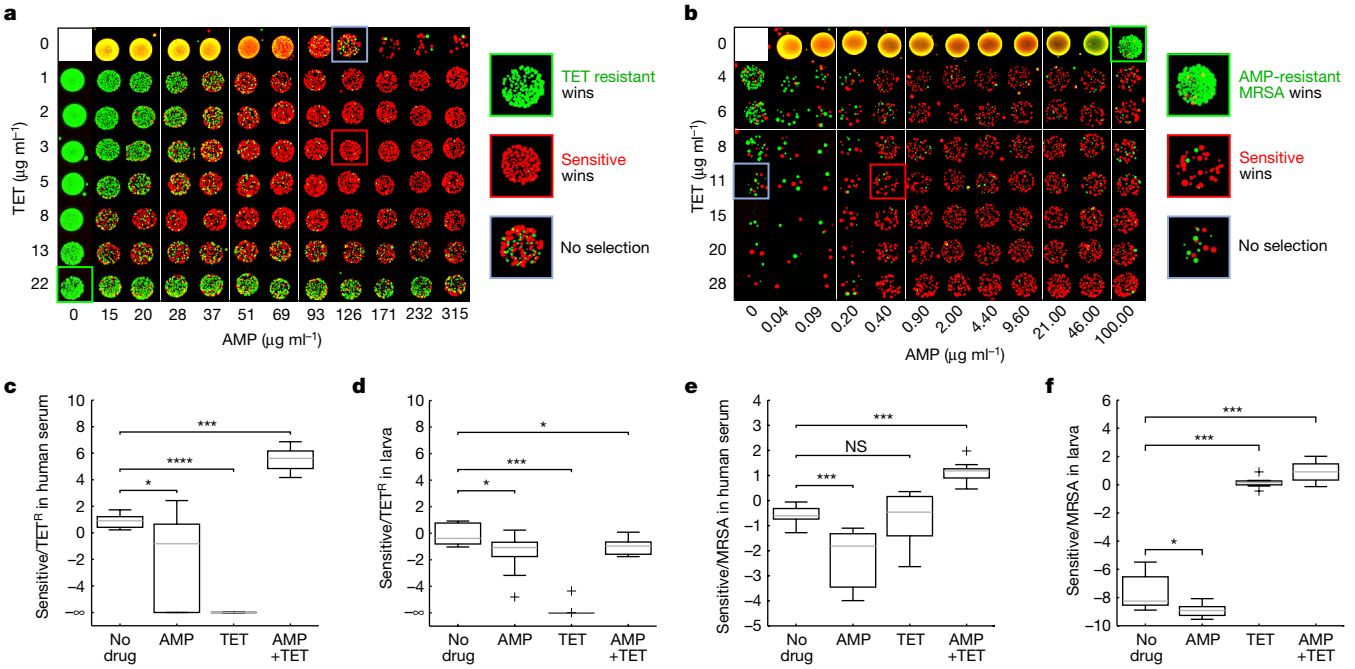

Fig. 3 | Reciprocal suppressive drug combination selects against antibiotic resistance to either of the single drugs. a,**b**, Microplating images of surviving colonies after 8 h competition of equally mixed sensitive (ATCC 29213) versus evolved TET-resistant strains (**a**; Sensitive, red; TET resistant, green) and sensitive versus MRSA strains (**b**; sensitive (red); AMP-resistant MRSA (green)) in a two-dimensional gradient of TET and AMP. Insets: magnified images under the selective drug alone (green; TET (**a**); AMP (**b**)), the non-selective drug (blue; AMP (**a**); TET (**b**)) and the combination (red; selecting against TET^R (**a**); selecting against MRSA (**b**)). **c**,**e**, The $\log_2$-transformed ratio of the survival of the sensitive (green) and TET-resistant (**c**; TET^R, red) or MRSA (**e**; red) strains after competing them in human serum with TET (2 μg ml^{-1} (**c**); 50 μg ml^{-1} (**e**)), AMP (150 μg ml^{-1} (**c**); 35 μg ml^{-1} (**e**)) and with TET + AMP for 8 h. Two strains measured in five experiments per condition. Statistical analysis was performed using two-sided Mann–Whitney *U*-tests; from left to right, $P = 0.0207$, $P = 0.0001$ and $P = 0.0002$ (**c**); $P = 0.0006$, $P = 0.9097$ and $P = 0.0002$ (**e**). **d**,**f**, The $\log_2$-transformed ratio of the survival of the sensitive and TET-resistant or MRSA strains measured 8 h after inoculation into larvae treated with TET (1.5 μg ml^{-1} (**d**); 50 μg ml^{-1} (**f**)), AMP (38 μg ml^{-1} (**d**); 100 μg ml^{-1} (**f**)) or TET–AMP. For **d**, $n = 10$ TrueLarvae per condition. For **f**, $n = 8$ AROLarvae per condition. For **d** and **f**, statistical analysis was performed using two-sided Mann–Whitney tests; from left to right, $P = 0.0173$, $P = 0.0001$ and $P = 0.0211$ (**d**); $P = 0.0207$, $P = 0.0002$ and $P = 0.0002$ (**f**). The box plots show the median (centre line); the upper and lower quartiles (box limits); and the maximum and minimum values (whiskers).

Focusing on the combination of TET and ampicillin (AMP) (a reciprocal suppressive pair for long-term clearance; Fig. 1c), we competed our sensitive ancestral strain with either a strain that is resistant to TET (TET evolved) (Methods, Fig 3a and Extended Data Fig. 9c,d) or a strain that is resistant to cell-wall inhibitors (methicillin-resistant *Staphylococcus aureus* (MRSA) (Fig. 3b and Extended Data Fig. 9e–g), or we compared the sensitive strain with and without an inducible β-lactamase (Methods and Extended Data Fig. 9a,b)). By contrasting the survival of the drug-sensitive and drug-resistant strains after 8 h of exposure to a two-dimensional concentration gradient of TET and AMP, we found that, under an extended region of the two-drug concentration space, the long-term survival of the resistant strains was much lower compared with the sensitive strain (10-fold to 100-fold) (Extended Data Fig. 9a–g). These selection inversions resulted from the interaction itself; there was no selection against the resistant strains under any of the single treatments. Selection against each of the single-drug-resistant mutants also occurred in competition within human serum (Fig. 3c,e and Extended Data Fig. 9h) and selection against MRSA was even observed within the *G. mellonella* infection model (in TET–AMP (Fig. 3f) as well as in MIN–AMP (Methods and Extended Data Fig. 9i). However, note that in this in vivo environment, even the single drugs, TET and MIN, showed selection against the MRSA strain (Fig. 3f and Extended Data Fig. 9i; perhaps reflecting suppressive interactions of these drugs with natural antimicrobial peptides in vivo)[50]. Selection against TET-resistant mutants did not occur within larvae, possibly due to the effect of oxygen depletion on the action of β-lactams[51] and due to competition for resources within larvae (Fig. 3d).

Reverse effect of resistance inhibition

Finally, given the ability of suppressive drug pairs to select against AMP resistance, we examined the effect of supplementing these drug combinations with a β-lactamase inhibitor. β-Lactamase inhibitors are commonly used together with β-lactams to increase treatment efficacy against strains carrying the β-lactamase enzyme. We measured the long-term survival of a β-lactamase-mediated AMP-resistant strain (Methods) as a function of increasing doses of avibactam, a known β-lactamase inhibitor, in the presence of three different clearance-suppressive drug combinations (AMP combined with TET, CLI or FUS; Fig. 4). Consistent with these combinations selecting against AMP resistance, we found that adding avibactam to these clearance-suppressive combinations decreased rather than increased the long-term clearance efficacy against the β-lactam-resistant strain (Fig. 4 and Extended Data Fig. 10a–d). Thus, in the presence of clearance-suppressive drug combinations, a β-lactamase inhibitor jeopardizes, rather than facilitates, treatment efficacy.

Discussion

By systematically quantifying the growth inhibition and killing dynamic of individual drugs and drug combinations at cidal, clinically relevant concentrations, we found that reciprocal suppressive interactions emerge in prolonged treatment efficacy. In contrast to shorter-term drug effects and conventional wisdom, drug efficacy is reduced rather than increased as more drugs are combined. These strong suppressive clearance interactions are suggestive of induced

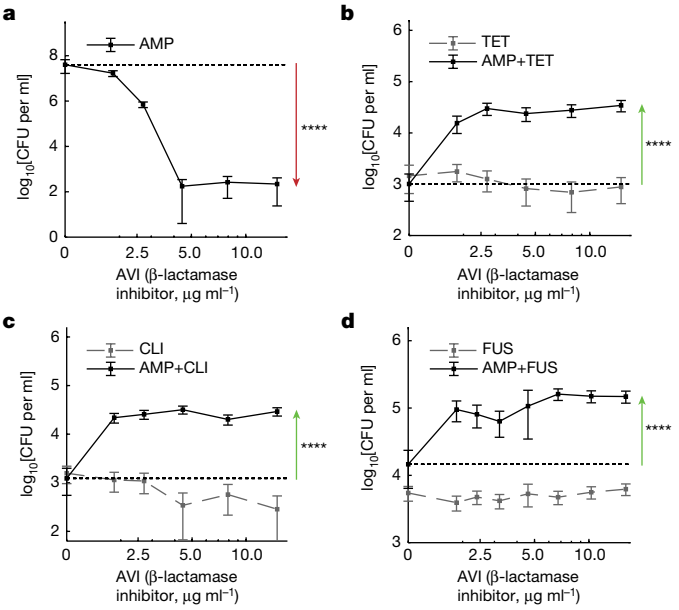

Fig. 4 | Supplementing clearance suppressive combinations with avibactam, a β-lactamase inhibitor, decreased rather than increased the long-term clearance efficacy against a β-lactamase-carrying strain. a, As expected, the killing efficacy of AMP at fixed dosage (0.5 μg ml^{-1}) is enhanced by the addition of an increasing dosage of avibactam (AVI). **b**–**d**, By contrast, the treatment efficacy is reduced rather than enhanced when avibactam is added to a combination of AMP (0.5 μg ml^{-1}) with a fixed dosage of TET (**b**; 20 μg ml^{-1}), CLI (**c**; 10 μg ml^{-1}) or AMP (**d**; 0.4 μg ml^{-1}) with FUS (**d**, 20 μg ml^{-1}). No AMP controls show that this inverted effect of AVI is mediated by the interaction among AMP and these protein-synthesis inhibitors (grey dashed lines). The error bars represent 95% confidence intervals calculated from the colony counts of one sample by the Poisson's model. Statistical analysis was performed using *z*-tests based on the Poisson-derived confidence intervals; $P < 10^{-10}$.

persistence in the presence of specific drug combinations. Indeed, adding persistence-targeting, weakly metabolism-dependent drugs, such as mitomycin C and daptomycin, can completely restore the efficacy of these otherwise suppressive drug mixes, explaining the clinical success of drug combinations involving these drugs[52]. Clinicians should also be cautious in relying on growth inhibition phenotypes as a guide for prescribing drug combination therapies, as drug combinations with high inhibitory efficacy, such as TET and cell wall inhibitors[53], may have reduced long-term efficacy. The lack of correlation between growth inhibition interactions and long-term clearance interactions is consistent with earlier observations[14] and we hypothesize that it may stem from the differential dependencies of these interactions on the physiology of the population majority and population heterogeneity, respectively[14,26]. Furthermore, owing to these clearance-suppressive drug interactions, adding β-lactamase inhibitors can, counterintuitively, jeopardize the long-term clearance efficacy of the drug combinations against β-lactamase-carrying resistant strains, cautioning against certain clinically prescribed combinations such as the combination of macrolides or doxycycline with amoxicillin/clavulanate for the treatment of community-acquired pneumonia[54,55]. At the same time, reciprocal suppressive drugs also open up new opportunities for designing treatment regimens that are inherently selective against resistance to any one of their individual agents. However, note that further study will be needed to more fully understand the mechanism of drug-combination-induced bacterial persistence[56,57], and the range of possible evolutionary paths that may enable bacteria to escape selection against resistance[12]. Although the results proved to be robust to changes in drug doses, external conditions and strain backgrounds, for assessing any clinical relevance, it will also be important to determine the extent to which they apply in other bacterial species, and in mammalian in vivo models. However, as drugs could interact in profoundly different ways in terms of their effect on growth and early and late population survival, our study underscores the importance of systematically quantifying the long-term clearance efficacy of drug combinations for guiding the design of multidrug treatments that may better prevent the evolution of drug resistance.

Online content

Any methods, additional references, Nature Research reporting summaries, source data, extended data, supplementary information, acknowledgements, peer review information; details of author contributions and competing interests; and statements of data and code availability are available at https://doi.org/10.1038/s41586-022-05260-5.

1. Yeh, P., Tschumi, A. I. & Kishony, R. Functional classification of drugs by properties of their pairwise interactions. *Nat. Genet.* **38**, 489–494 (2006).
2. Ocampo, P. S. et al. Antagonism between bacteriostatic and bactericidal antibiotics is prevalent. *Antimicrob. Agents Chemother.* **58**, 4573–4582 (2014).
3. Brochado, A. R. et al. Species-specific activity of antibacterial drug combinations. *Nature* **559**, 259–263 (2018).
4. Beppler, C. et al. When more is less: emergent suppressive interactions in three-drug combinations. *BMC Microbiol.* **17**, 107 (2017).
5. Yilancioglu, K. & Cokol, M. Design of high-order antibiotic combinations against *M. tuberculosis* by ranking and exclusion. *Sci. Rep.* **9**, 11876 (2019).
6. Russ, D. & Kishony, R. Additivity of inhibitory effects in multidrug combinations. *Nat. Microbiol.* **3**, 1339–1345 (2018).
7. Katzir, I., Cokol, M., Aldridge, B. B. & Alon, U. Prediction of ultra-high-order antibiotic combinations based on pairwise interactions. *PLoS Comput. Biol.* **15**, e1006774 (2019).
8. Tekin, E. et al. Prevalence and patterns of higher-order drug interactions in *Escherichia coli*. *NPJ Syst. Biol. Appl.* **4**, 31 (2018).
9. Cokol, M., Kuru, N., Bicak, E., Larkins-Ford, J. & Aldridge, B. B. Efficient measurement and factorization of high-order drug interactions in *Mycobacterium tuberculosis*. *Sci. Adv.* **3**, e1701881 (2017).
10. Zimmer, A., Katzir, I., Dekel, E., Mayo, A. E. & Alon, U. Prediction of multidimensional drug dose responses based on measurements of drug pairs. *Proc. Natl Acad. Sci. USA* **113**, 10442–10447 (2016).
11. Kulesa, A., Kehe, J., Hurtado, J. E., Tawde, P. & Blainey, P. C. Combinatorial drug discovery in nanoliter droplets. *Proc. Natl Acad. Sci. USA* **115**, 6685–6690 (2018).
12. Liu, J., Gefen, O., Ronin, I., Bar-Meir, M. & Balaban, N. Q. Effect of tolerance on the evolution of antibiotic resistance under drug combinations. *Science* **367**, 200–204 (2020).
13. Hofsteenge, N., van Nimwegen, E. & Silander, O. K. Quantitative analysis of persister fractions suggests different mechanisms of formation among environmental isolates of E. coli. *BMC Microbiol.* **13**, 25 (2013).
14. Zheng, E. J., Stokes, J. M. & Collins, J. J. Eradicating bacterial persisters with combinations of strongly and weakly metabolism-dependent antibiotics. *Cell Chem. Biol.* **27**, 1544–1552 (2020).
15. Murillo, O. et al. Efficacy of high doses of daptomycin versus alternative therapies against experimental foreign-body infection by methicillin-resistant *Staphylococcus aureus*. *Antimicrob. Agents Chemother.* **53**, 4252–4257 (2009).
16. Mascio, C. T. M., Alder, J. D. & Silverman, J. A. Bactericidal action of daptomycin against stationary-phase and nondividing *Staphylococcus aureus* cells. *Antimicrob. Agents Chemother.* **51**, 4255–4260 (2007).
17. Kwan, B. W., Chowdhury, N. & Wood, T. K. Combatting bacterial infections by killing persister cells with mitomycin C. *Environ. Microbiol.* **17**, 4406–4414 (2015).
18. Lewis, K. Persister cells, dormancy and infectious disease. *Nat. Rev. Microbiol.* **5**, 48–56 (2007).
19. Nathan, C. & Cars, O. Antibiotic resistance—problems, progress, and prospects. *N. Engl. J. Med.* **371**, 1761–1763 (2014).
20. Langford, B. J. et al. Bacterial co-infection and secondary infection in patients with COVID-19: a living rapid review and meta-analysis. *Clin. Microbiol. Infect.* **26**, 1622–1629 (2020).
21. Mwangi, M. M. et al. Tracking the in vivo evolution of multidrug resistance in *Staphylococcus aureus* by whole-genome sequencing. *Proc. Natl Acad. Sci. USA* **104**, 9451–9456 (2007).
22. Snitser, O. et al. Ubiquitous selection for *mecA* in community-associated MRSA across diverse chemical environments. *Nat. Commun.* **11**, 6038 (2020).
23. Peyrusson, F. et al. Intracellular *Staphylococcus aureus* persisters upon antibiotic exposure. *Nat. Commun.* **11**, 2200 (2020).
24. Garzoni, C. & Kelley, W. L. Return of the Trojan horse: intracellular phenotype switching and immune evasion by *Staphylococcus aureus*. *EMBO Mol. Med.* **3**, 115–117 (2011).
25. Balaban, N. Q., Merrin, J., Chait, R., Kowalik, L. & Leibler, S. Bacterial persistence as a phenotypic switch. *Science* **305**, 1622–1625 (2004).
26. Brauner, A., Fridman, O., Gefen, O. & Balaban, N. Q. Distinguishing between resistance, tolerance and persistence to antibiotic treatment. *Nat. Rev. Microbiol.* **14**, 320–330 (2016).
27. Fisher, R. A., Gollan, B. & Helaine, S. Persistent bacterial infections and persister cells. *Nat. Rev. Microbiol.* **15**, 453–464 (2017).

28. Cottarel, G. & Wierzbowski, J. Combination drugs, an emerging option for antibacterial therapy. *Trends Biotechnol.* **25**, 547–555 (2007).
29. Yeh, P. J., Hegreness, M. J., Aiden, A. P. & Kishony, R. Drug interactions and the evolution of antibiotic resistance. *Nat. Rev. Microbiol.* **7**, 460–466 (2009).
30. Tyers, M. & Wright, G. D. Drug combinations: a strategy to extend the life of antibiotics in the 21st century. *Nat. Rev. Microbiol.* **17**, 141–155 (2019).
31. Baym, M., Stone, L. K. & Kishony, R. Multidrug evolutionary strategies to reverse antibiotic resistance. *Science* **351**, aad3292 (2016).
32. Singh, N. & Yeh, P. J. Suppressive drug combinations and their potential to combat antibiotic resistance. *J. Antibiot.* **70**, 1033–1042 (2017).
33. Chait, R., Craney, A. & Kishony, R. Antibiotic interactions that select against resistance. *Nature* **446**, 668–671 (2007).
34. Jacqueline, C. et al. In vitro activity of linezolid alone and in combination with gentamicin, vancomycin or rifampicin against methicillin-resistant *Staphylococcus aureus* by time-kill curve methods. *J. Antimicrob. Chemother.* **51**, 857–864 (2003).
35. Jawetz, E., Gunnison, J. B., Speck, R. S. & Coleman, V. R. Studies on antibiotic synergism and antagonism; the interference of chloramphenicol with the action of penicillin. *AMA Arch. Intern. Med.* **87**, 349–359 (1951).
36. Zeiler, H. J. Evaluation of the in vitro bactericidal action of ciprofloxacin on cells of *Escherichia coli* in the logarithmic and stationary phases of growth. *Antimicrob. Agents Chemother.* **28**, 524–527 (1985).
37. Zinner, S. H., Provonchee, R. B., Elias, K. S. & Peter, G. Effect of clindamycin on the in vitro activity of amikacin and gentamicin against gram-negative bacilli. *Antimicrob. Agents Chemother.* **9**, 661–664 (1976).
38. Brown, T. H. & Alford, R. H. Antagonism by chloramphenicol of broad-spectrum beta-lactam antibiotics against *Klebsiella pneumoniae*. *Antimicrob. Agents Chemother.* **25**, 405–407 (1984).
39. Bahl, D. et al. In vitro activities of ciprofloxacin and rifampin alone and in combination against growing and nongrowing strains of methicillin-susceptible and methicillin-resistant *Staphylococcus aureus*. *Antimicrob. Agents Chemother.* **41**, 1293–1297 (1997).
40. Johansen, H. K. Antagonism between penicillin and erythromycin against *Streptococcus pneumoniae* in vitro and in vivo. *J. Antimicrob. Chemother.* **46**, 973–980 (2000).
41. Bollenbach, T., Quan, S., Chait, R. & Kishony, R. Nonoptimal microbial response to antibiotics underlies suppressive drug interactions. *Cell* **139**, 707–718 (2009).
42. Lorian, V. *Antibiotics in Laboratory Medicine* (Lippincott Williams & Wilkins, 2005).
43. O'Grady, F. & Greenwood, D. Interactions between fusidic acid and penicillins. *J. Med. Microbiol.* **6**, 441–450 (1973).
44. Stone, L. K. et al. Compounds that select against the tetracycline-resistance efflux pump. *Nat. Chem. Biol.* **12**, 902–904 (2016).
45. Jawetz, E., Gunnison, J. B. & Coleman, V. R. The combined action of penicillin with streptomycin or chloromycetin on enterococci in vitro. *Science* **111**, 254–256 (1950).
46. Lobritz, M. A. et al. Antibiotic efficacy is linked to bacterial cellular respiration. *Proc. Natl Acad. Sci. USA* **112**, 8173–8180 (2015).
47. Klepser, M. E., Nicolau, D. P., Quintiliani, R. & Nightingale, C. H. Bactericidal activity of low-dose clindamycin administered at 8- and 12-hour intervals against *Staphylococcus aureus*, *Streptococcus pneumoniae*, and *Bacteroides fragilis*. *Antimicrob. Agents Chemother.* **41**, 630–635 (1997).
48. Zahedi Bialvaei, A., Rahbar, M., Yousefi, M., Asgharzadeh, M. & Samadi Kafil, H. Linezolid: a promising option in the treatment of Gram-positives. *J. Antimicrob. Chemother.* **72**, 354–364 (2017).
49. Maier, L. et al. Unravelling the collateral damage of antibiotics on gut bacteria. *Nature* **599**, 120–124 (2021).
50. Lázár, V. et al. Antibiotic-resistant bacteria show widespread collateral sensitivity to antimicrobial peptides. *Nat. Microbiol.* **3**, 718–731 (2018).
51. Léger, L. et al. β-Lactam exposure triggers reactive oxygen species formation in *Enterococcus faecalis* via the respiratory chain component DMK. *Cell Rep.* **29**, 2184–2191 (2019).
52. Blackman, A. L., Rubin, E. C., Broadbent, E. K. & Brade, K. D. Updates on combination therapy for methicillin-resistant *Staphylococcus aureus* bacteremia. *Curr. Infect. Dis. Rep.* **22**, 28 (2020).
53. Liu, C. et al. Clinical practice guidelines by the infectious diseases society of america for the treatment of methicillin-resistant *Staphylococcus aureus* infections in adults and children: executive summary. *Clin. Infect. Dis.* **52**, 285–292 (2011).
54. Matisko, M. W. & Bissada, N. F. Short-term sequential administration of amoxicillin/clavulanate potassium and doxycycline in the treatment of recurrent/progressive periodontitis. *J. Periodontol.* **64**, 553–558 (1993).
55. Butt, S. & Swiatlo, E. Treatment of community-acquired pneumonia in an ambulatory setting. *Am. J. Med.* **124**, 297–300 (2011).
56. Fung, D. K. C., Barra, J. T., Schroeder, J. W., Ying, D. & Wang, J. A shared alarmone-GTP switch underlies triggered and spontaneous persistence. Preprint at *bioRxiv* https://doi.org/10.1101/2020.03.22.002139 (2020).
57. Miller, C. et al. SOS response induction by beta-lactams and bacterial defense against antibiotic lethality. *Science* **305**, 1629–1631 (2004).

Methods

Strains and plasmids

The *S. aureus* sp. Rosenbach (ATCC 29213) strain was transformed with either a DsRed (pHC48, sarAP1_DsRed, CHL^R) or a sGFP fluorescent reporter gene (pCM29, sarAP1_sGFP, CHL^R) under a constitutive promoter[58] (antibiotic-sensitive *S. aureus*). To test for generality and for counter-selection experiments, the MW2 *S. aureus* strain[59] was similarly transformed with these two plasmids (MRSA) (Fig. 3b,e,f and Extended Data Fig. 9e–i). A β-lactamase-inducible plasmid was constructed by amplifying the *blaZ* gene from *Enterococcus faecalis* (ATCC 49757) and cloning by Gibson assembly under the TET-inducible promoter of the pG+off plasmid[60]. This plasmid was transformed into the sensitive *S. aureus* strain to form the AMP^R strain in the presence of 0.05 μM anhydrotetracycline (Fig. 4 and Extended Data Figs. 9a,b and 10a–d). Laboratory evolution was performed according to a previously established protocol to evolve the antibiotic-sensitive *S. aureus* strain to TET[61]. A resistant clone with the highest TET minimal inhibitory concentration (25-fold increase compared with the ancestral strain) was transformed with either the DsRed or the GFP plasmid and used in the experiments of Fig. 3a,c,d and Extended Data Fig. 9c,d (TET^R). Fresh antibiotic solutions were prepared from powder stocks (Sigma-Aldrich, Cayman chemical, AdooQ Bioscience) on a monthly basis, filter-sterilized and kept at −20 °C until use.

Quantifying bacterial survival under antibiotic exposure

We adapted a high-throughput cell-viability assay[44] in which bacterial cultures were exposed to single or multiple drugs in 96-well assay plates and their viability across time was quantified by microplating and colony counting. Specifically, these experiments were performed in 6 steps. (1) Preparation of bacterial stocks. Single colonies of the GFP and DsRed fluorescently labelled sensitive *S. aureus* strains were isolated and grown overnight in LB supplemented with 10 μg ml^{-1} CHL (to maintain the plasmid) at 37 °C, 250 rpm. Overnight cultures were diluted 1:5,000 and grown to an optical density at 600 nm (OD_{600}) of 0.25. These cultures were concentrated by centrifugation and small aliquots of 50 μl containing ~2.2×10^9 cells were frozen in glycerol (stored at −80 °C). (2) Preparing assay plates with antibiotics. Deep 96-well plates were filled with 600 μl LB and supplemented with single or multiple antibiotics using an automated digital dispenser (D300e, Tecan). At least two replicate wells were randomly distributed for each condition. (3) Antibiotic exposure. For each biological replicate, frozen cultures of the GFP and DsRed strains were thawed and mixed at a 1:1 ratio, diluted 1:250 in 25 ml LB and incubated for 40 min at 37 °C and 250 rpm. These co-growing bacterial cultures were then aliquoted into the 96-well deep-well antibiotic plates (150 μl culture; total volume of 750 μl) at a low inoculum density of about 10^6–10^7 CFU per ml to minimize the risk of pre-existing resistant mutants and prevent nutrient depletion (Extended Data Fig. 10j–m; the growth of the resistant strain was not limited in the supernatant of the FOX regimes that kill the sensitive strain (>1 μg ml^{-1}) but not the resistant strain (<3.8 μg ml^{-1}), especially in the wells in which the starting density of the sensitive strain was initially low (<10^7); this result indicates that nutrient depletion is negligible during our killing assay starting with a 10^7–10^6 initial population size). This inoculum density follows recommended clinical testing standards for killing assays[42]. No-cell and no-antibiotic wells were designated on each plate to control for contamination (2–5 of the wells in each plate). (4) Microplating assay for quantification of bacterial viability (colony-forming units (CFU)). At fixed time points after antibiotic exposure at 37 °C and 250 rpm (0, 0.25, 0.5, 1 and 1.5 h for the early-killing assay; and 0, 0.5, 1, 2, 4 and 8 h for the long-term clearance assay), small aliquots (10–150 μl) were taken from each well, and fivefold serial diluted for plating. The 8 h time point was the last time point for sampling as the clearance efficacy of many of the single drugs (Extended Data Fig. 5) already reached the detection limit of our assay (1 colony in 7 μl volume plated; ~140 CFU per ml; extending beyond 8 h requires larger plating volumes, which cannot be done in microplates). Large-volume experiments for the two chosen drug pairs showed robustness of the clearance interactions even at 24 h (Extended Data Fig. 6c). For the 8 h clearance assay, in which cell viability declined substantially, we also plated the undiluted culture (dilutions of 5^n, where $n = 0–4$) and therefore added a wash step by centrifugation and resuspension to remove the drugs (three washes with 800 μl PBS at 4,000 rpm for 10 min). For the killing-assay, in which cell viability was higher, an initial dilution of at least 50× was used, precluding the washing step (final dilutions of 50×5^n, where $n = 0–2$). Small microdrops (7 μl) from each dilution were then carefully microplated (Gilson 96-channel plate master) in one to four technical replicates onto omnitray single-well (Greiner) plates filled with 45 ml of agar with 0.2× diluted LB and incubated for 24 h at 37 °C. The diluted LB was used to limit the substrate availability on the agar thereby allowing the growth of many small colonies on a relatively small surface area[62]. (5) Imaging. After incubation, the agar plates were imaged for GFP (excitation:470/30; emission: 540/50) and DsRed (excitation: 590/30; emission 641/75) with a custom-made automated macroscope device[63]. (6) Detection of resistance. At the last time point, 15 μl aliquots from each well of the assay plates were also inoculated into a 96-well plate with 200 μl liquid LB containing, in each well, the same antibiotic concentrations of the assay plates and incubated overnight at 37 °C at 250 rpm. After incubation, the growing cultures ($OD_{600} > 0.2$), indicating resistant cells, were excluded from further analysis. Overall, our data included ~15,000 microdrops: $n = 2$ biologically independent strains (DsRed, GFP) measured in 585 drug conditions (28 singles (1×, 2× dose) and 91 pairs), 5 × 36 singles (1×, 2×, 3×, 4×, 5× and 6× dose), 5 × 57 multidrug mixes); 1–5 timepoints; 2 time ranges (short-term and long-term killing), at least 2 independent replicates and 4 to 8 platings (dilutions + technical replicates).

Automated image analysis

The number of red and green colonies in each microplating spot was counted using a custom Python script[64], implementing the following steps. (1) The GFP and DsRed microplating images (one for each microplating spot) were contrast-enhanced and noise-reduced (mean shift pyramid). (2) These enhanced GFP and DsRed images were thresholded (mahotas.otsu), yielding two corresponding binary images. (3) An exact Euclidean distance transform was used to yield a distance matrix of each pixel to its nearest zero pixel (scipy.ndimage.distance_transform_edt). (4) Local peaks in the distance matrix (skimage.feature.peak_local_max) were clustered into connected components (nearest neighbours, scipy.ndimage.label) to yield labelled feature arrays. (5) These feature arrays were used as seeds to the watershed algorithm to segregate the colonies (skimage.morphology.watershed). (6) Thresholding on the basis of the size and circularity of the colonies was applied to remove very tiny colonies or merged spots. (7) Microplating spots where the colonies merged extensively or with colonies that were too dense to reliably count were designated uncountable (over 100 colonies per spot). (8) For each given culture and time point, the colony counts at dilutions at which there was no uncountable plating were used to evaluate the CFU per ml (total number of colonies in all of the countable dilutions divided by total culture volume plated). Our high-throughput viability assay was highly reproducible, showing good agreement among biological replicates (Extended Data Fig. 10e–h). Co-cultures of GFP/DsRed strains enabled us to: (1) increase the sensitivity of the colony-detection algorithm—different colour colonies can be more easily distinguished even if they grow at close proximity; (2) spot low-frequency antibiotic-resistant mutants that manifest as red-only or green-only colonies on the agar spot where two identical strains labelled with different fluorescent tags; (3) conduct competition experiments in which the sensitive and resistant strains were labelled differentially (see below).

Calculating early-killing and clearance interaction scores between drug pairs

Early-killing and long-term clearance directional interaction scores (DIS) among pairwise combinations of the 14 antibiotics were quantified based on the fraction of surviving cells S after short (average of the 1 and 1.5 h time points; the killing delay was almost always shorter than half an hour across the different conditions indicating that the average cell survival after 1 and 1.5 h is an effective killing score that combines both the killing rate and drug action delay; Extended Data Fig. 10i) and long (8 h time point; the choice of 8 h incubation time is often used[25,26,65,66], although note that longer times are used in some of the studies[13,67,68]) antibiotic exposures, respectively. For each drug A of the 14 antibiotics, a fixed cidal concentration ($A_{1\times}$) was chosen on the plateau phase of the dose–response curves (Extended Data Fig. 2a and Supplementary Table 1). For each drug pair A and B, cell survival under each drug alone at these chosen concentrations ($S_{A(1\times)}$, $S_{B(1\times)}$), in double these concentrations ($S_{A(2\times)}$, $S_{B(2\times)}$) and in a mix of the two drugs ($S_{A(1\times)+B(1\times)}$) was evaluated. Then, the effect of drug B on drug A ($DIS_{B\to A}$) and the effect of drug A on drug B ($DIS_{A\to B}$) were defined on the basis of a comparison of the joint drug action $S_{A(1\times)+B(1\times)}$ with four reference idealized values. Specifically, the effect of drug B on A was defined as no-killing ($S_{A(1\times)+B(1\times)} = 1$, $DIS_{B\to A} = 4$), no effect ($S_{A(1\times)+B(1\times)} = S_{A(1\times)}$, $DIS_{B\to A} = 3$), adding B is the same as adding A ($S_{A(1\times)+B(1\times)} = S_{A(2\times)}$, $DIS_{B\to A} = 2$) and enhanced killing ($S_{A(1\times)+B(1\times)}$ below detection limit, $DIS_{B\to A} = 1$). For $S_{A(1\times)+B(1\times)}$ between these reference values, $DIS_{B\to A}$ was determined by a linear interpolation between the two flanking reference values (Fig. 1b,c and Extended Data Fig. 1f). The effect of drug A on B was similarly quantified.

Calculating early-killing and long-term clearance interaction scores between multidrug combinations

To quantify early-killing and long-term clearance interactions among all of the possible multidrug combinations of six drugs ($n = 63$), we measured the fraction of surviving cells after short (average of the 1 h and 1.5 h time points) and long antibiotic exposure (8 h), respectively. Cell viability was quantified for each of the six drugs separately when applied at a fixed cidal concentration ($A_{1\times}$, the same as in the pairwise screen), at double ($A_{2\times}$), triple ($A_{3\times}$), four times ($A_{4\times}$), five times ($A_{5\times}$) and six times ($A_{6\times}$) of the $A_{1\times}$ concentration and for all of the possible combinations of the six drugs (for example, $A_{1\times} + B_{1\times}$, $A_{1\times} + C_{1\times}$, $B_{1\times} + C_{1\times}$, $A_{1\times} + B_{1\times} + C_{1\times}$ and so on, for a total of 57 multidrug mixes). We then calculated an interaction score (IS) for all of the possible pairs of drug mixes (for example, A + B, A + C, B + C, AB + C, A + BC, AC + B; total of 301 drug mix pairs). For each given pair of drug mixes (M1 and M2), the survival under the combined treatment of these drug mixes (S_{M1+M2}) was contrasted with four reference values representing idealized cases of no-killing ($S_{M1+M2} = 1$, IS = 4), lowest single-agent effect (LSA, $S_{M1+M2} = \max[S_{M1}, S_{M2}]$, IS = 3), highest single agent effect (HSA, $S_{M1+M2} = \min[S_{M1}, S_{M2}]$, IS = 2) and enhanced killing (S_{M1+M2} below detection limit, IS = 1). For S_{M1+M2} between these reference values, IS was determined by a linear interpolation between the two flanking reference values (Fig. 2c,d and Extended Data Figs. 7d,e and 8b,d).

Competition of fluorescently tagged drug-sensitive and drug-resistant strains

The antibiotic-sensitive (ATCC 29213) strain was competed with either the MRSA strain, or the laboratory evolved TET-resistant strain (TET^R). Differentially labelled cultures were mixed at a 1:1 ratio and our high-throughput cell-viability assay (as described in 'Quantifying bacterial survival under antibiotic exposure') was applied to quantify cell counts after an 8 h treatment with a two-dimensional concentration gradient of TET and AMP. The experiment was repeated with fluorescent-marker-swapped strains, showing no marker-specific effect on survival (Fig. 3a–c,e and Extended Data Fig. 9c–h).

Testing the robustness of reciprocal suppression clearance interactions to different media

The clearance interactions between two representative reciprocal suppressive drug combinations (CLI–CLO and FOX–TET) (Fig. 1c and Extended Data Fig. 5) were measured in different media including Luria–Bertani (LB), brain–heart infusion (BHI), tryptic soy broth (TSB) and human serum (Extended Data Fig. 6b). Antibiotic concentrations were adjusted to give a similar clearance efficacy in each condition (source data for Extended Data Fig. 6). Our high-throughput cell-viability assay was applied with minor modifications: for each biological replicate, the frozen cultures of GFP and DsRed were thawed and mixed at 1:1 ratio, diluted 1:250 dilution in 5 ml of the appropriate medium (LB, BHI, TSB, in case of the serum experiment LB was used) in culture tubes and incubated for 20 min at 37 °C and 250 rpm. The cell-viability assay, microplating and automated image analyses were then performed as described above.

Testing the robustness of reciprocal suppression clearance interactions to longer incubation times

To compare drug interactions after 8 h and 24 h incubation time, we repeated the cell-viability assay of two representative reciprocal suppressive drug combinations (CLI–CLO; TET–FOX) (Fig. 1c and Extended Data Fig. 5) using a standard plating technique on regular Petri dishes (Extended Data Fig. 6c). Culture tubes were filled with 2 ml LB medium supplemented with single or multiple antibiotics. For each independent replicate, frozen cultures of GFP and DsRed were thawed and mixed at a 1:1 ratio, diluted 1:250 in 5 ml LB in a culture tubes and incubated for 15 min at 37 °C and 250 rpm. These co-growing bacterial cultures were then aliquoted into each tube (135 µl culture) at a low inoculum density of about 10^6–10^7. After incubation for 8 h and 24 h at 37 °C and 250 rpm, 400 µl samples were taken, washed three times with 1 ml PBS and resuspended in 200 µl PBS. Then, 100 µl samples were spread from each dilution onto LB agar Petri dishes and incubated for 24 h at 37 °C. The plate imaging and automated colony counting were performed according to the same steps as described above.

Testing the robustness of reciprocal suppression clearance interactions to bacterial physiological state in a plasmid-less strain

The clearance interaction was measured between CLI and CLO starting from two different biologically independent *S. aureus* cultures in different physiological conditions (Extended Data Fig. 6d; exponential growing and late growing phase). Frozen aliquots of these cultures were prepared by taking two single colonies of the plasmid-less sensitive *S. aureus* strain, growing overnight in LB, then diluted 1:5,000 and grown to either $OD_{600} = 0.1$ or OD = 0.8. Then, both of these cultures were concentrated by centrifugation and small aliquots of 50 µl containing ~2×10^9 cells were frozen in glycerol (−80 °C). For each independent replicate, these frozen cultures were thawed, diluted 1:250 in 2 ml LB and incubated for 15 min at 37 °C and 250 rpm. A standard plating technique was applied (as described above) to measure cell viability after incubation for 24 h in human serum supplemented with the single drugs or the combination. Plates were imaged using the Canon EOS T3i camera followed by manual colony counting.

Clearance efficacy and competition in the *G. mellonella* infection model

Larvae of the *G. mellonella* at their final instar stage were used to assess the clearance efficacy of drug combinations. Larvae were either purchased from UK BioSystem Technology (TRUELarvae) or from the Israel Agricultural Research Organization, Volcani Institute (AROLarvae). Antibiotic stock solutions were freshly prepared and diluted in PBS to the required concentration. Drugs and fluorescently tagged *S. aureus* (~10^7) bacterial suspensions (with chloramphenicol resistance) were

premixed in PBS on ice and administered by injecting 30–50 µl into the haemocoel through one of the final pair of prolegs using a Hamilton precision syringe. Larvae were randomly allocated to experimental groups. The untreated control larvae were injected with the same bacterial strain culture in the absence of drugs. Chosen drug concentrations, specified in the corresponding figure caption of each experiment, were below the toxicity level but high enough to decrease the bacteria cell number (killing regime). The larvae were then placed into Petri dishes and incubated at 37 °C for 8 h. After incubation, the larvae were frozen for 5 min, decontaminated by 70% ethanol and homogenized using a hand-held homogenizer in 5 ml PBS. The number of surviving *S. aureus* cells was determined by plating 5- or 10-fold dilution series of the homogenized larvae onto LB agar plates supplemented with 10 µg ml^{-1} chloramphenicol to prevent contamination from larva microbiomes. The plates were then incubated at 37 °C for 24 h and fluorescent colonies were counted and imaged (as described above) (Figs. 1d (bottom) and 3d,f and Extended Data Fig. 6f–i).

Measuring growth inhibition under 2D concentration gradients

Growth inhibition of all the pairwise combinations of the 14 antibiotics (n = 91; Extended Data Figs. 1a–e and 3) was measured on the sensitive *S. aureus* (ATCC 29213) according to a previously established experimental protocol[50]. First, for each drug A, a concentration gradient covering its effective range was defined as $D_A(k) = IC10_A \times w^{k-1}$, where $D_A(k)$ is the dosage of the drug at dilution number k, $w = (IC90_A/IC10_A)^{1/3}$ is the dilution factor, $IC10_A$ and $IC90_A$ are the concentrations of A drug resulting in 10% and 90% inhibition, respectively; and k ranges from 1 to 8 (such that the lowest concentration is $D_A(1)$ = IC10 and the highest concentration is $D_A(8)$=IC90 × w^4). Then, for each pair of drugs A and B, a 96-well microplate was filled with 150 µl LB, supplemented (D300e Tecan digital dispenser) with (1) a 2D concentration gradient of A and B defined by mixing their single-drug gradients at seven different ratios: (i/8 × $D_A(k)$, (8 − i)/8 × $D_B(k)$), where i = 1–7 and k = 1–8 (total of 56 wells), (2) a 12-step dilution series of each of the two drugs alone ($D_A(k)$ and $D_B(k)$, where k varies −3 to 8, total of 24 wells), (3) bacteria-free contamination control (2 wells), (4) no-drug control (6 wells). These assay plates were then inoculated with the sensitive *S. aureus* at 10^5 cells per ml and incubated for 18 h in 37 °C, shaken at 250 rpm. After incubation, the OD_{600} (BioTek Synergy 2) was measured as the basis for calculating the interaction scores between the two drugs.

Calculating growth-inhibition interaction score

For each pair of the 14 antibiotics, the OD of their 2D drug assay plates was used to quantify directional growth-inhibition interaction scores (DGIS). First, the OD was background-subtracted and normalized to the no-drug control wells. Second, a polynomial surface model was fitted (Loess fit[69] to these normalized OD values to determine the concentration of each drug leading to 90% growth inhibition ($IC90_A$, $IC90_B$) as well as the 90% growth inhibition isobole (IC90 isobole). To quantify directional growth-inhibition interaction scores, we considered the distance from the origin to the IC90 isobole along two straight lines representing fixed A:B ratios (in IC90 units) of 1:3 for effect of drug A on drug B (A→B) and 3:1 for effect of drug B on drug A (B→A). These two distances were then interpolated relative to the corresponding distances associated with the intersection of these fixed-ratio lines with 4 reference isobole lines representing extreme synergy (no drug, DGIS = 1), Loewe's dosage additivity (DGIS = 2), antagonism (highest single agent (HSA), DGIS = 3) and strong suppression (2× HSA, DGIS = 4) (Extended Data Figs. 1a–e and 3).

Reporting summary

Further information on research design is available in the Nature Research Reporting Summary linked to this article.

Data availability

All data supporting the findings of this study are provided as Source Data. The raw data files, including the microplating images with the bacterial colonies, are available in a public data repository (https://osf.io/wh62f/). Source data are provided with this paper.

Code availability

Custom script developed for the study was deposited in a public data repository (https://osf.io/wh62f/).

58. Malone, C. L. et al. Fluorescent reporters for *Staphylococcus aureus*. *J. Microbiol. Methods* **77**, 251–260 (2009).
59. Baba, T. et al. Genome and virulence determinants of high virulence community-acquired MRSA. *Lancet* **359**, 1819–1827 (2002).
60. Lartigue, M.-F. & Bouloc, P. A tetracycline-inducible expression vector for *Streptococcus agalactiae* allowing controllable gene expression. *J. Microbiol. Methods* **96**, 16–18 (2014).
61. Lázár, V. et al. Bacterial evolution of antibiotic hypersensitivity. *Mol. Syst. Biol.* **9**, 700 (2013).
62. Liu, X., Wang, S., Sendi, L. & Caulfield, M. J. High-throughput imaging of bacterial colonies grown on filter plates with application to serum bactericidal assays. *J. Immunol. Methods* **292**, 187–193 (2004).
63. Chait, R., Shrestha, S., Shah, A. K., Michel, J.-B. & Kishony, R. A differential drug screen for compounds that select against antibiotic resistance. *PLoS ONE* **5**, e15179 (2010).
64. Lazar, V. Project—diminished *Staphylococcus aureus* clearance under drug combinations. *OSFHOME* https://doi.org/10.17605/OSF.IO/WH62F (2022)
65. Lechner, S., Lewis, K. & Bertram, R. *Staphylococcus aureus* persisters tolerant to bactericidal antibiotics. *J. Mol. Microbiol. Biotechnol.* **22**, 235–244 (2012).
66. Allison, K. R., Brynildsen, M. P. & Collins, J. J. Metabolite-enabled eradication of bacterial persisters by aminoglycosides. *Nature* **473**, 216–220 (2011).
67. Bartell, J. A. et al. Bacterial persisters in long-term infection: emergence and fitness in a complex host environment. *PLoS Pathog.* **16**, e1009112 (2020).
68. Singh, R., Barry, C. E. 3rd & Boshoff, H. I. M. The three RelE homologs of *Mycobacterium tuberculosis* have individual, drug-specific effects on bacterial antibiotic tolerance. *J. Bacteriol.* **192**, 1279–1291 (2010).
69. Cleveland, W. S., Grosse, E. & Shyu, W. M. in *Statistical Models in S* (eds Chambers, J. M. & Hastie, T. J.) Ch. 8, 608 (Wadsworth & Brooks/Cole, 1992).

Acknowledgements We thank R. Gross, E. Shaer-Tamar, I. Yelin, M. Datta, D. Ross and M. Lukacisinova for reading the manuscript and for comments and suggestions; the members of S. Walker's laboratory for bacterial strains; A. Horswill for the fluorescence plasmids; I. Yelin for the β-lactamase plasmid; and D. Ment for the *G. mellonella* larvae. V.L. was supported by a postdoctoral fellowship from the Human Frontier Science Program Organization (LT001011/2017-L) and in part by Technion Postdoctoral Fellowship. This work was supported in part by the US National Institutes of Health grant R01-GM081617, the ISRAEL SCIENCE FOUNDATION (grant no. 455/19) and the European Research Council FP7 ERC grant 281891 (to R.K.).

Author contributions V.L. and R.K. conceived and designed the study. V.L. performed all of the in vitro experiments. V.L., O.S., R.K. and D.B. designed the experiments in the larvae infection model. V.L. and O.S. performed the experiments in the larvae infection model. V.L. and R.K. analysed the data and wrote the paper.

Competing interests The authors declare no competing interests.

Additional information

Supplementary information The online version contains supplementary material available at https://doi.org/10.1038/s41586-022-05260-5.

Correspondence and requests for materials should be addressed to Roy Kishony.

Peer review information *Nature* thanks the anonymous reviewers for their contribution to the peer review of this work.

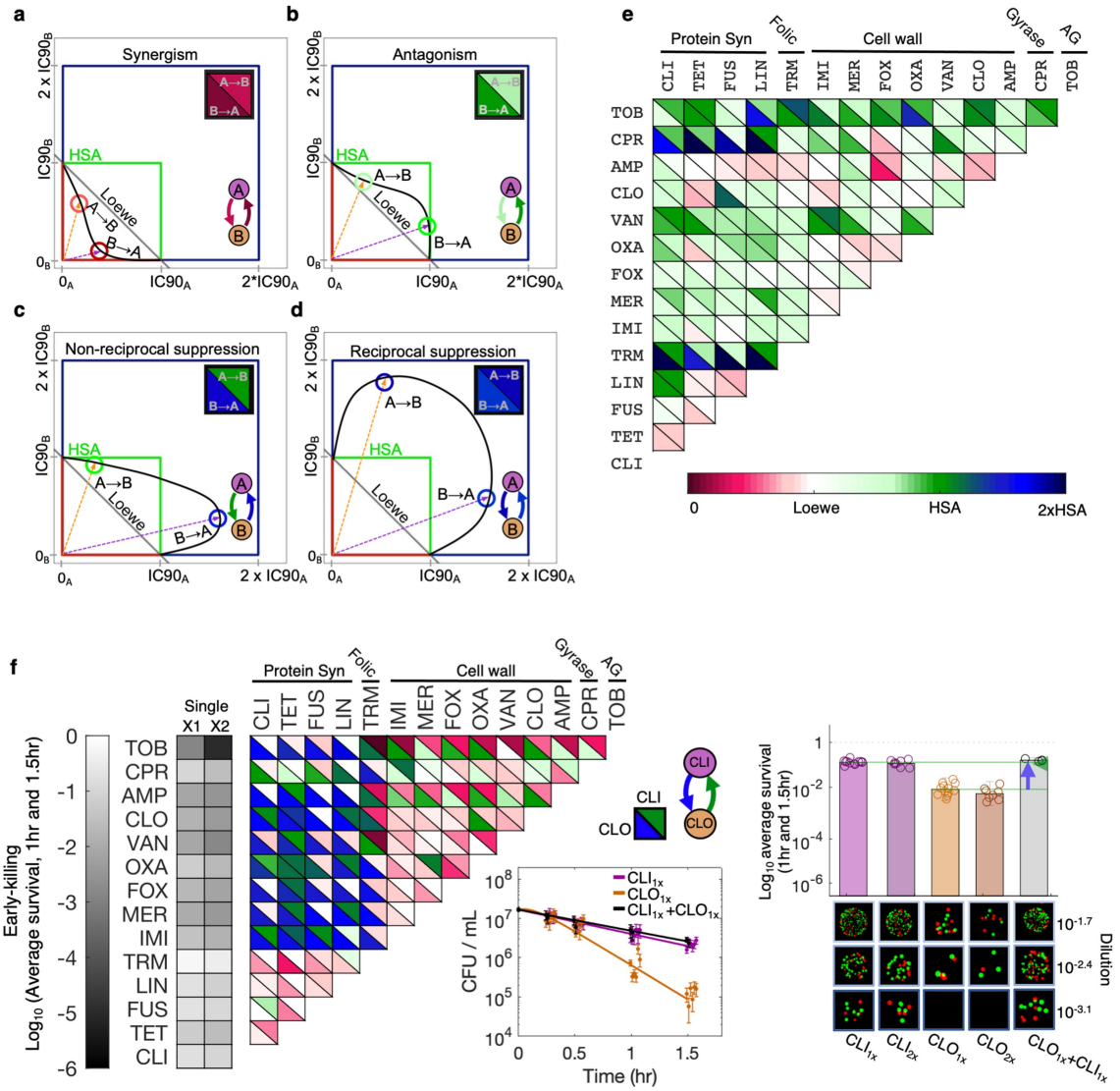

Extended Data Fig. 1 | Systematic mapping of pairwise growth-inhibition and early-killing interactions. a–d, Definition of directional growth-inhibition interaction scores. Measuring the growth as the final optical density (OD) in a 2-D gradient of drugs A and B after 18-hour of incubation, we define the concentration of each drug leading to 90% growth inhibition ($IC90_A$, $IC90_B$) as well as the 90% growth inhibition isobole (IC90 isobole, black line). To quantify bi-directional interactions, we consider the distance from the origin to the IC90 isobole along two straight lines representing fixed A:B ratios (in IC90 units) of 1:3 for effect of drug A on drug B (A→B, dashed orange) and 3:1 for effect of drug B on drug A (B→A, dashed magenta). These two distances are then interpolated relative to the corresponding distances associated with the intersection of these fixed-ratio lines with 4 reference isobole lines representing extreme synergy (red), Loewe's dosage additivity (grey), antagonism (Highest Single Agent, HSA, green) and strong suppression (blue). The four panels illustrate four representative examples of synergism (a), antagonism (b), non-reciprocal suppression (c) and reciprocal suppression (d). **e**, Measurements of the directional growth-inhibition interaction scores for pairwise combinations of 14 antibiotics. Upper (lower) triangles show the interaction score for the effect of the drugs in the row (column) on the drugs in the column (row). **f**, Measurements of directional interaction scores for pairwise combinations of 14 antibiotics in early-killing (2 biologically independent strains measured in $A_{1\times}$, $A_{2\times}$, and $A_{1\times} + B_{1\times}$ at 6, 4, 2 experiments, respectively). Upper (lower) triangles show the interaction score for the effect of the drugs in the row (column) on the drugs in the column (row). Insets show the killing curves and the average survival fractions following short (1 and 1.5-hour) treatment with a representative suppressive drug combination. For each treatment, representative micro-plating images of one of the replicates are shown. Error bars represent 95% confidence intervals calculated from the colony counts of the experiments by the Poisson's model (f, middle panel) or 2x s.e.m. (f, right panel).

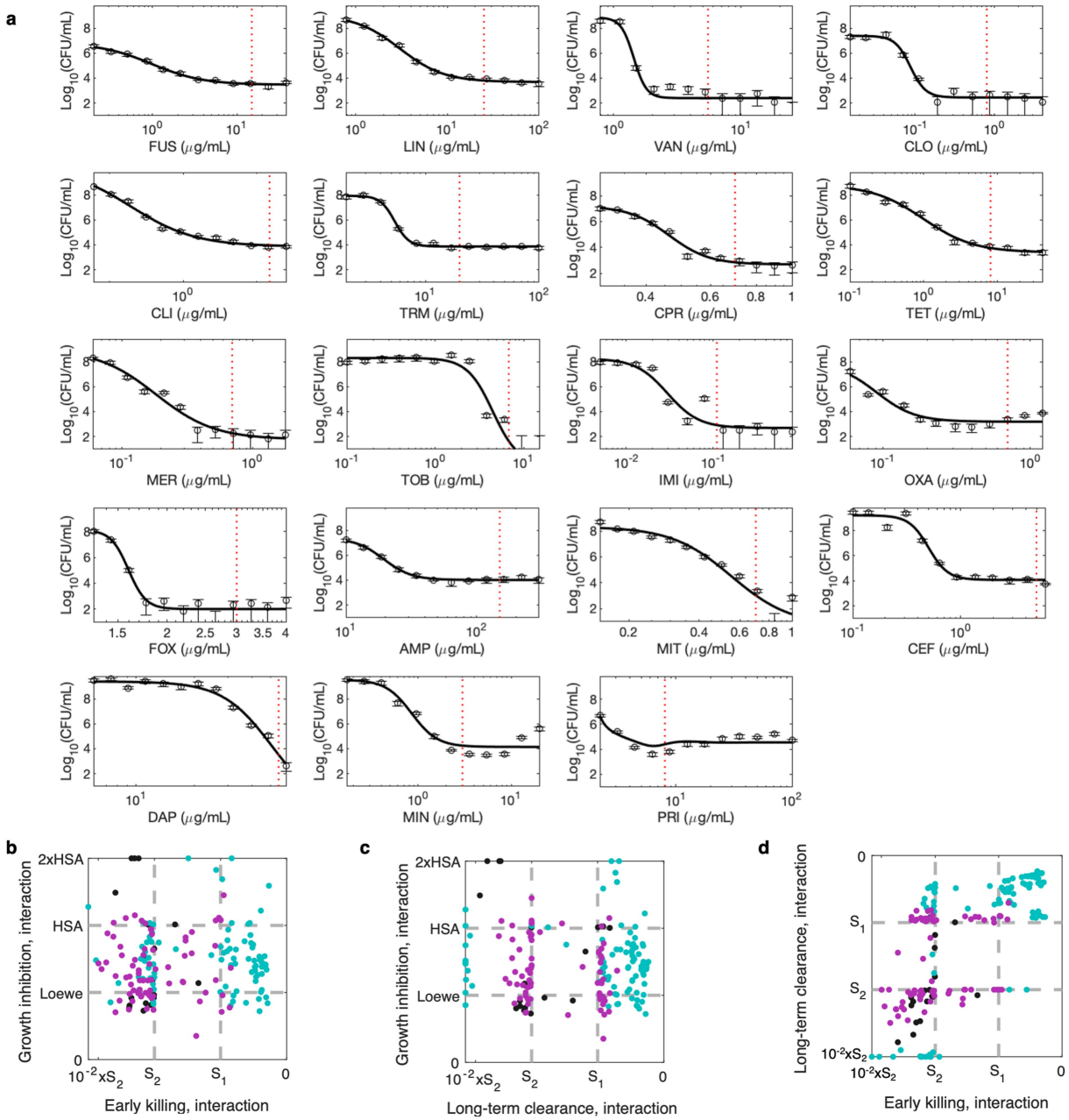

Extended Data Fig. 2 | a, The dose response curves of 19 drugs. Cell viability (CFU/ml) measured following 8-hour exposure to different concentrations of 19 drugs. Hill function fit indicated (note though a slight non monotonic behaviour for some of the antibiotics). The fixed cidal concentration chosen for each drug is indicated as a red line ("x1", Methods, Fig. 1b, Supplementary Table 1). The cell viability of 2 biologically independent strains were measured over each drug. Error bars represent 95% confidence intervals calculated from the colony counts by the Poisson's model . **b–d, Lack of correlation between directional interactions of growth-inhibition and early-killing or long-term clearance**. The directional interaction scores for all the pairwise combination of 14 antibiotics (n = 182, coloured by three different drug-pair groups: (1) black, pairs of classically static (CS) drug pairs; (2) purple, pairs of cidal drug pairs; (3) cyan, combining a cidal and CS drugs ranged from synergistic to antagonistic and suppression. There is a lack of correlation between growth-inhibition interactions (Extended Data Fig. 1e) and early-killing interactions (Extended Data Fig. 1f) seen for all drug pairs (b; Rho:0.04) and within each of the three drug-pair groups (CS pairs, Rho:0.01; cidal pairs, Rho:0.01; CS-cidal pairs, Rho:−0.15); as well as between growth-inhibition and long-term-killing interactions (Fig. 1c) between all drug pairs (c, Rho:−0.02) and within each of the three drug-pair groups (CS pairs, Rho:−0.1; cidal pairs, Rho:−0.13; CS-cidal pairs, Rho:−0.18). While there is a significant strong correlation (d, Rho:0.73, P-value:4.5×10^{-32}) between early-killing and long-term clearance interactions seen for all drug pairs and within each of the three drug-pair groups (CS pairs, Rho:0.69, P-value:10^{-3}; cidal pairs, Rho:0.47, P-value:3.4×10^{-5}; CS-cidal pairs, Rho:0.61, P-value:1.9×10^{-10}) indicating that the long-term effect of the drug combinations can be predicted, to a good extent, from the early-killing efficacy. Spearman's test was applied.

Extended Data Fig. 3 | Pairwise interactions in growth inhibition. For each pair of the 14 antibiotics (91 pairs), *S. aureus* (ATCC 29213) growth was measured following 18-hour exposure to 2-D dosage gradients of two drugs (normalized final OD, size of black dots). A polynomial surface model was fitted (Loess fit; R stats) to these normalized OD values represented by the isoboles for growth inhibitions of 30%, 60% and 90%. The 90% inhibition isobole was contrasted with four reference isobole lines representing extreme synergy (red), Loewe's dosage additivity (grey), antagonism (green) and strong suppression (blue). The distance of the 90% inhibition line from these reference isoboles was measured along two linear lines of fixed A:B drug dosage ratios of 1:3 and 3:1 (in IC90 units, dashed magenta, and orange lines), representing the effect of drug A on drug B and the effect of drug B on drug A, respectively. The unit of the A and B axis is µg/ml.

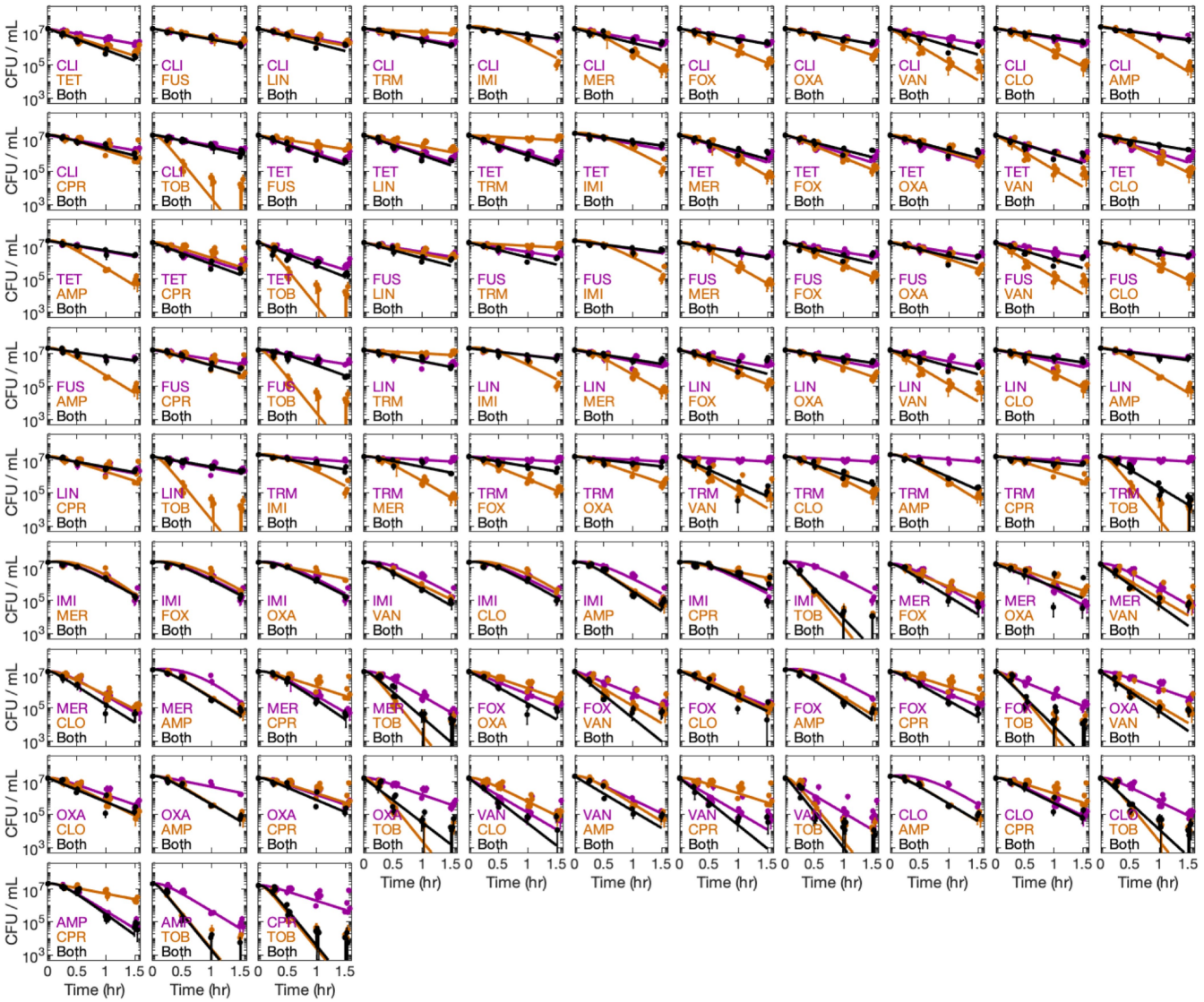

Extended Data Fig. 4 | Pairwise interactions in early-killing. Decline in cell viability is measured as colony forming unit per ml (CFU/ml) along 90 min following exposure to each of the 14 drugs when applied individually (orange and magenta) and when applied, at the same doses, in pairwise combinations (black). The line represents the least square fit of the viability measurement over time to $\exp(-L(k+\mu)(e^{-t/L}-1)-kt)$ where t is time, μ is the measured growth rate in absence of drug (=1.4/hour), and L and k are two fitted parameters representing an effective time delay for drug action, and the killing rate, respectively (2 biologically independent strains measured in $A_{1\times}$, $A_{2\times}$, and $A_{1\times}+B_{1\times}$ at 6, 4, 2 experiments, respectively). Error bars represent 95% confidence intervals of the experiments calculated from the colony counts by the Poisson's model.

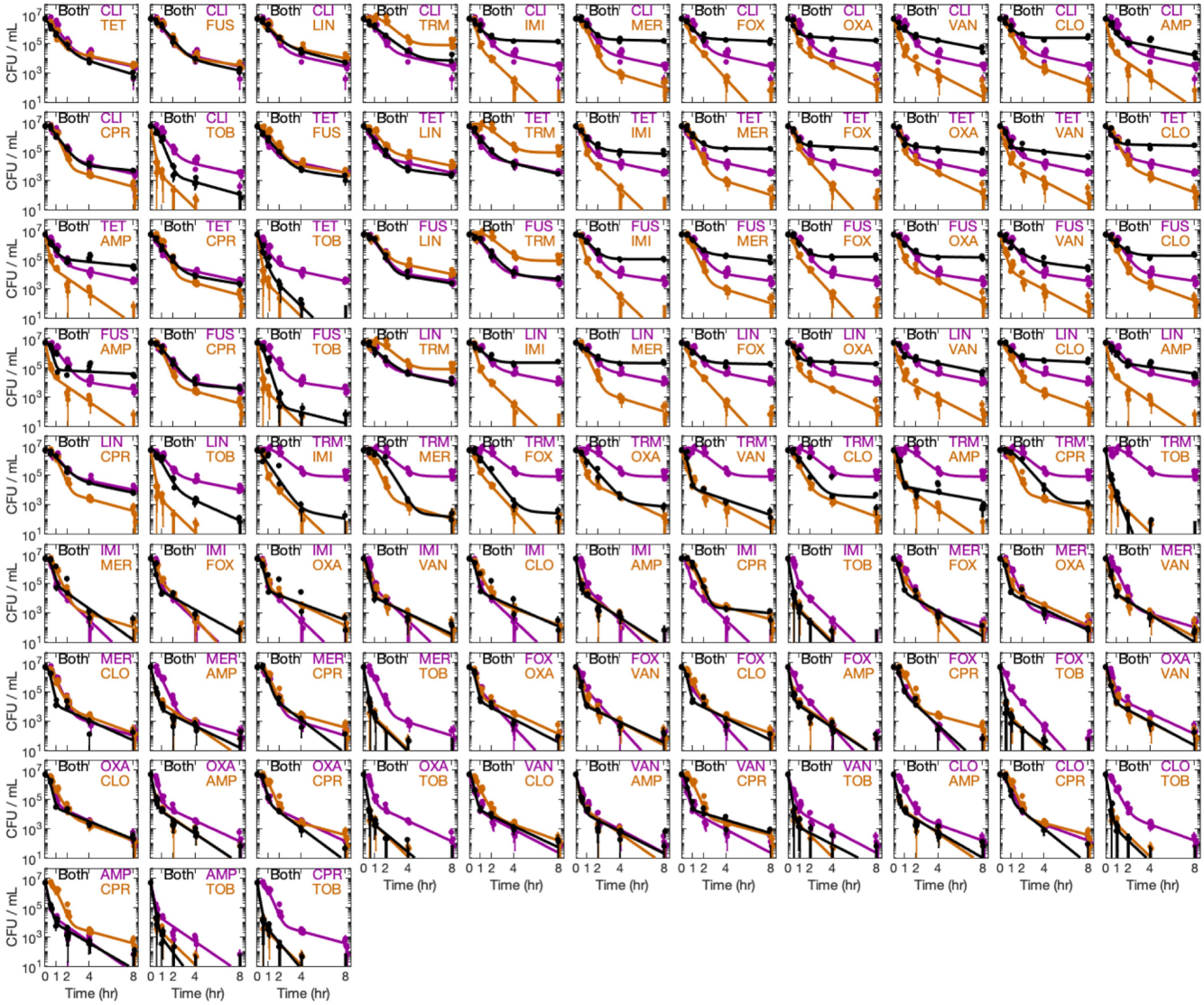

Extended Data Fig. 5 | Pairwise interactions in long-term killing. Decline in cell viability is measured as colony forming unit per ml (CFU/ml) along 8 h following exposure to each of the 14 drugs when applied individually (orange and magenta) and when applied, at the same doses, in pairwise combinations (black). The line represent the least square fit of the CFU measurement over time to $(1\text{-}f_p)\exp(\text{-}L(k_n+\mu)(e^{-t/L}\text{-}1)\text{-}k_n t)+f_p\exp(\text{-}k_p t)$ where t is time, μ is the measured growth rate in absence of drug (=1.4/hour), and L, f_p, k_n and k_p are four fitted parameters representing an effective time delay for drug action, the fraction of persistent cells, and the killing rates of the normal and the persistent cells, respectively (2 biologically independent strains measured in $A_{1\times}$, $A_{2\times}$, and $A_{1\times}+B_{1\times}$ at 6, 4, 2 experiments, respectively). Error bars represent 95% confidence intervals of the experiments calculated from the colony counts by the Poisson's model.

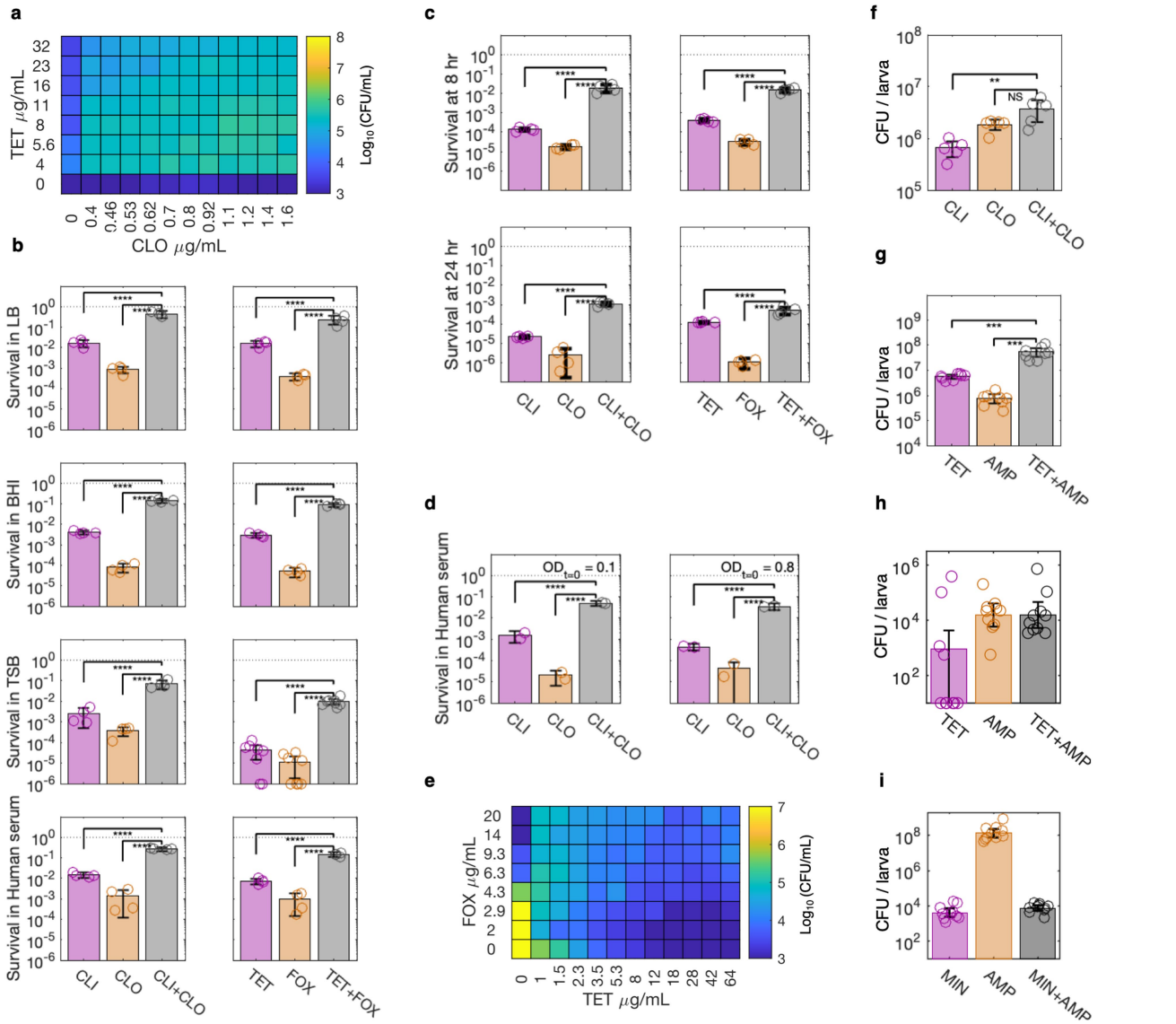

Extended Data Fig. 6 | Reciprocal suppressive interactions in long-term clearance efficacy are robust to changes in drug concentrations, growth environments, incubation time, bacterial physiological state, and strain backgrounds. a, Survival of the *S. aureus* (ATCC 29213) following 8-hour of exposure to cidal concentration of tetracycline and cloxacillin (TET-CLO) indicating robust reciprocal suppression over a wide range of drug concentrations (no bacteria well at 0,0 concentration point). **b**, Bacteria survival measured following 8-hour exposure to clindamycin-cloxacillin (CLI-CLO, left) or tetracycline-cefoxitin (TET-FOX, right) demonstrating strong reciprocal suppression in different media: Lauria Delbruck (LB), Brain-Heart Infusion (BHI), Tryptic Soy Broth (TSB), and human serum (2 biologically independent strains measured at 2 experiments; 4, for TET-FOX in TSB). **c**, Survival following exposure to CLI-CLO (10 μg ml^{-1}, 2 μg ml^{-1}) or TET-FOX (8 μg ml^{-1}, 4 μg ml^{-1}) in LB demonstrate reciprocal suppression both after 8-hour incubation (top, control) as well as after 24-hour (bottom; 2 strains measured at 2 replicates). **d**, Viability of 2 biologically independent strains in different physiological state (left, exponential growing state, OD = 0.1; right, late growing phase, OD = 0.8) was measured in 2 experiments following 8-hour exposure in human serum to CLI-CLO (50 μg ml^{-1}, 10 μg ml^{-1}; b-d **** P values < 10^{-10}; two tailed z-test). **e**, Reciprocal suppression is demonstrated in an unrelated, methicillin resistant *S. aureus* (MRSA, Methods). **f**, Viability of the sensitive strain measured 8-hour post inoculation into larvae treated with CLI-CLO (15 μg ml^{-1}, 40 μg ml^{-1}; n = 5 TRUElarvae per condition; left to right P values: 0.008, 0.103; Mann-Whitney test). **g**–**i**, Viability of the sensitive strain (GFP) measured 8-hour competition with the MRSA strain (g,i; DsRed) or with the TET^{R} strain (h; DsRed) within larvae treated with TET-AMP (g, 50 μg ml^{-1}, 100 μg ml^{-1}; h, 1.5 μg ml^{-1}, 38 μg ml^{-1}) or with CLI-AMP (i, 6 μg ml^{-1}, 6 μg ml^{-1}; g, n = 8 AROLarvae per condition, left to right P values: 1.5×10^{-4}, 1.5×10^{-4}, Mann-Whitney test, same experiment as in Fig. 3f; h, n = 10 TRUELarvae per condition, same experiment as in Fig. 3d; i, n = 10 TRUELarvae per condition, same experiment as in Extended Data Fig. 9i). Data are presented as mean +/− 95% confidence intervals (points on the axis are below the detection limit).

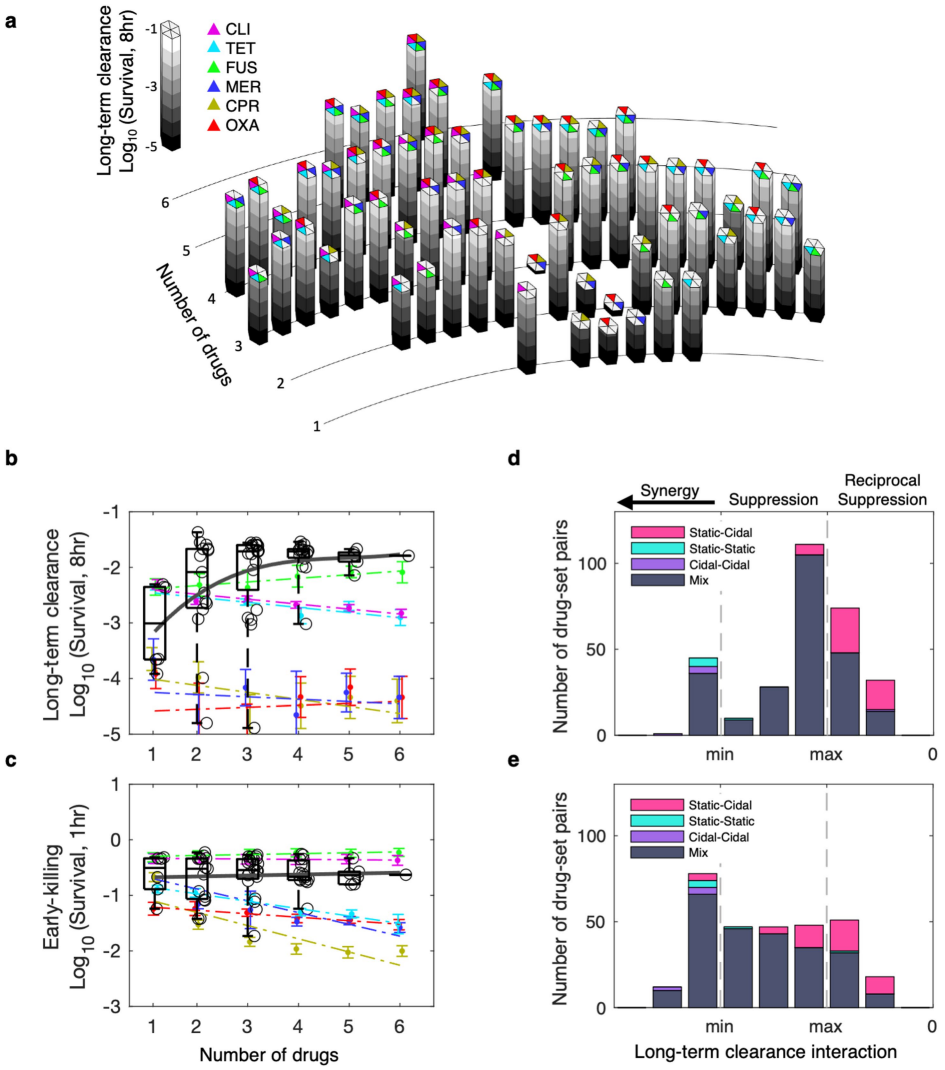

Extended Data Fig. 7 | Long-term clearance efficacy of multidrug combinations is reduced as more drugs are added. We repeated the Fig 2a experiment with newly prepared antibiotic and bacterial culture stocks and the results were consistent with our prior experiment (Fig. 2a). **a**, Bacterial survival following 8-hour of exposure to all possible combinations of 6 drugs (drug combinations are indicated by the colours at the top of the hexagonal columns, legend, Supplementary Table 1; 2 strains measured in 2 independent experiments) **b,c**, The survival fractions following long (8-hour, b) or short (1-hour, c) drug exposures as a function of the number of co-mixed drugs for all 6-drug combinations (average survival fraction of the two replicates of the 63 combinations; black circles; box-plots; centre line, median; box limits, upper and lower quartiles; whiskers, maximum and minimum values). Grey line shows quadratic fit. The coloured dots and coloured linear fit lines represent the efficacy of the single treatments as a function of increasing doses (from 1× to 6× of the dosage used in the combination; antibiotic color codes indicated in panel a). Data are presented as mean +/- 95% confidence intervals. **d,e**, The distribution of the clearance (d) and early-killing (e) interaction scores among all tested non-overlapping pairs of drug sets (for example, drug mix ABC is decomposed into AB+C, A+BC, AC+B; n = 301). The combined effect of the drug mix is shown relative to the minimum (min) and maximum (max) of the effect of the two drug sets (Methods). Drug mix pairs are classified as only cidal (purple), only classically static (CS; cyan), mix of all CS and all cidal (pink), pairs of mixed drug sets (mix, grey) .

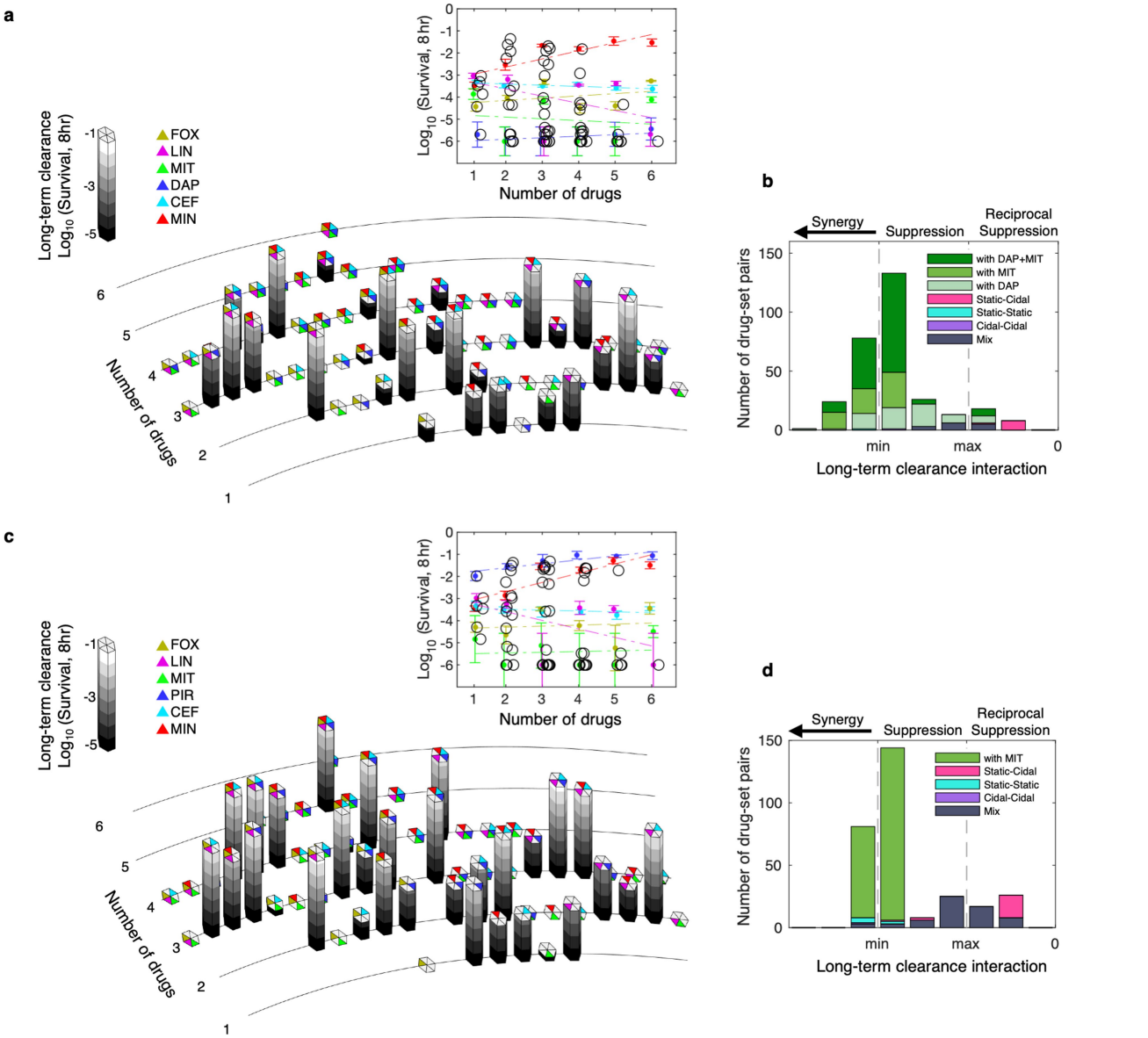

Extended Data Fig. 8 | The reduced clearance efficacy of multidrug mixes can be circumvented by specific persistence-targeting drugs. a,**c**, Bacterial survival following 8-hour of exposure to all possible combinations of 6 drugs including two persistence-targeting drugs (daptomycin, DAP; mitomycin C, MIT; drug combinations are indicated by the colours at the top of the hexagonal columns, legend, Supplementary Table 1; 2 biologically independent strains measured in 2 experiments). Inset: The survival fractions following long (8-hour) drug exposures as a function of the number of co-mixed drugs for all 6-drug combinations (n = 63 combinations; black circles). The coloured dots and coloured linear fit lines represent the efficacy of the single treatments as a function of increasing doses (from 1× to 6× of the dosage used in the combination; antibiotic color codes indicated in panel a; note though a slight non monotonic behaviour of the minocycline (MIN) and pristinamycine (PIR), possibly due to Eagle effect of the drugs). Data are presented as mean +/− 95% confidence intervals. **b**,**d**, The distribution of the clearance interaction scores among all tested non-overlapping pairs of drug sets (for example, drug mix ABC is decomposed into AB+C, A+BC, AC+B; n = 301). The combined effect of the drug mix is shown relative to the minimum (min) and maximum (max) of the effect of the two drug sets (Methods). Drug mix pairs are classified as only cidal (purple), only classically-static (CS; cyan), mix of all CS and all cidal (pink), pairs of mixed drug sets (mix, grey), or sets including DAP or MIT (green shades, legend). Persistence-targeting drugs strongly synergize the clearance efficacy of other drug mixes (Source Data for Fig. 2).

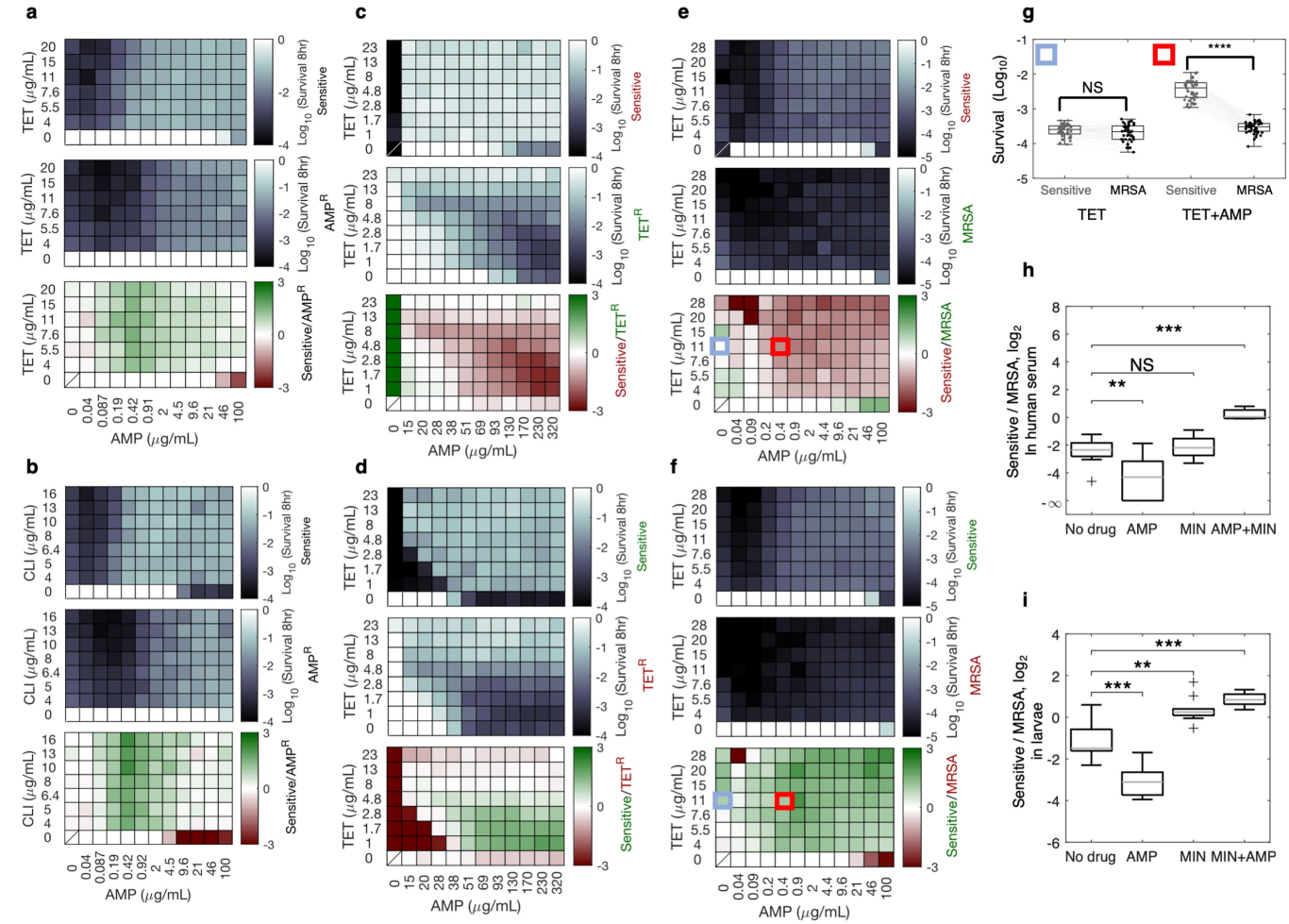

Extended Data Fig. 9 | Reciprocal suppressive drug combination selects against antibiotic resistance to either one of the single drugs. a,**b**, The survival fraction of the sensitive strain with and without an inducible β-lactamase (sensitive and AMP^R, respectively) was measured separately in two parallel experiments following 8-hour of exposure to a two-dimensional gradient of tetracycline (TET) and ampicillin (AMP) (e) or clindamycin (CLI) and AMP (f). **c**–**f**, Survival fraction measured after 8-hour competition of equally mixed sensitive (ATCC 29213, Methods) versus evolved tetracycline resistant strains (c, Sensitive, red; TET^R, green; d, Sensitive, green; TET^R, red) or MRSA strain (e, Sensitive, red; MRSA, green; f, Sensitive, green; MRSA, red) in two-dimensional gradient of tetracycline (TET) and ampicillin (AMP). The $\log_{10}$ of the ratio of the survival of the sensitive and resistant strains are shown in red and green color scale (at the bottom of each panel). **g**, Survival fraction of the sensitive (grey) and MRSA (black) strain following an 8-hour treatment with TET alone (11 μg ml^{-1}; blue box in panel e,f) and with TET-AMP mix (11 μg ml^{-1}, 0.4 μg ml^{-1}; red box in panel e,f; n = 24 replicates of sensitive-DsRed versus MRSA-GFP and n = 24 replicates of a corresponding marker-swap competition (P value = 3×10^{-17}, two sided Mann Whitney test). **h**–**i**, The $\log_2$ of the ratio of the survival of the sensitive (GFP) and MRSA (DsRed) resistant strains after competing them for 8-hour within human serum (h, 2 biologically independent strains measured in 5 independent experiments per condition; two sided Mann-Whitney test; from left to right P values: 0.0072, 0.65, 0.0002) or within larvae (i, n = 10 TRUE larvae per condition, two sided Mann-Whitney test; from left to right P values: 0.0004, 0.0017, 0.0002) with MIN (h, 40 μg ml^{-1}; i, 6 μg ml^{-1}), AMP (h, 35 μg ml^{-1}; i, 6 μg ml^{-1}) or MIN+AMP. Box-plots: centre line, median; box limits, upper and lower quartiles; whiskers, maximum and minimum value.

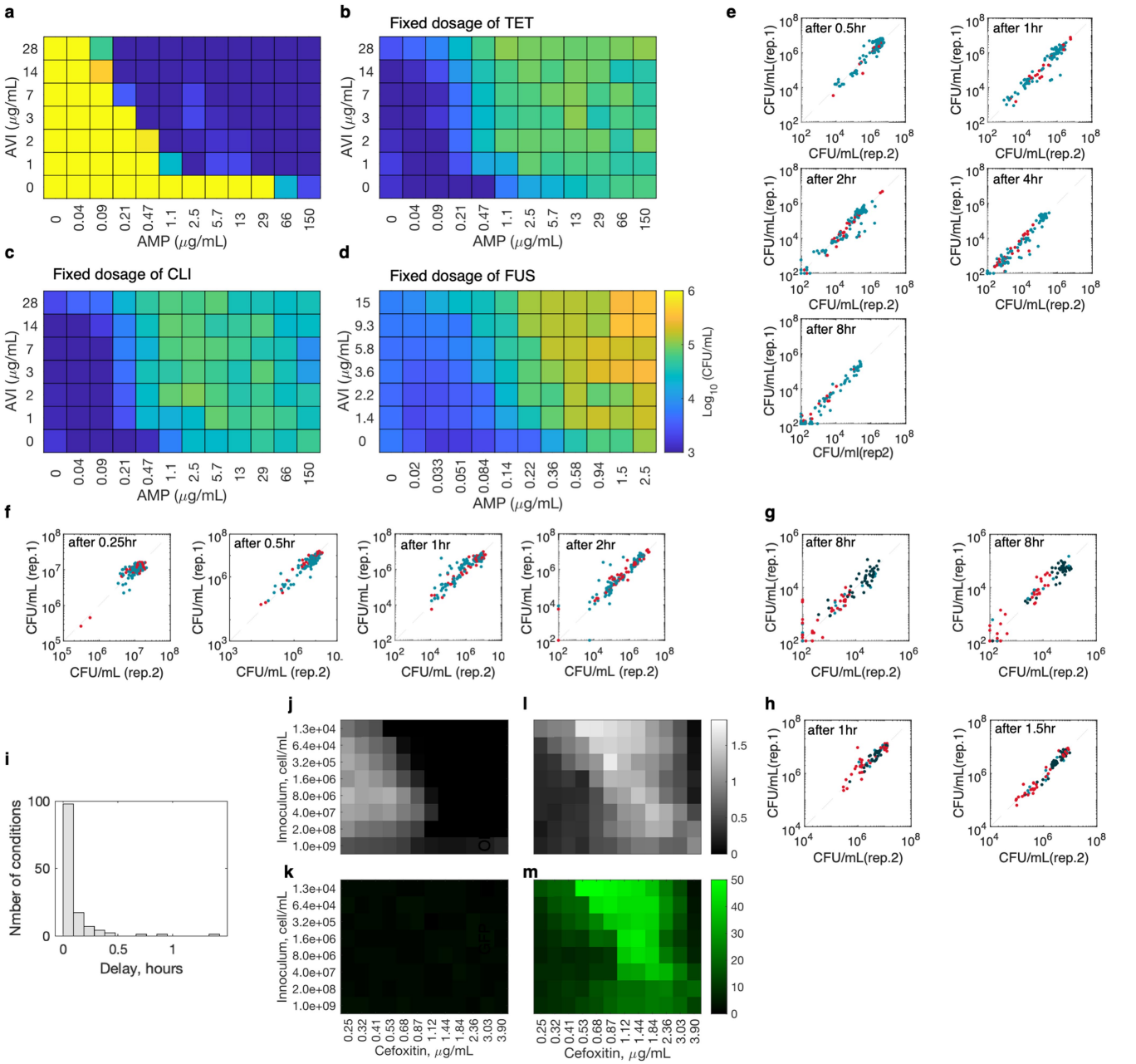

Extended Data Fig. 10 | a–d, Supplementing persistence-suppressive drug combinations with avibactam, a β-lactamase inhibitor, decreased rather than increased clearance efficacy against a β-lactam resistant strain. The clearance efficacy of ampicillin (AMP) is enhanced with the addition of increasing dosage of avibactam (AVI, a). In contrast, the treatment efficacy is reduced rather than enhanced when avibactam is added to the reciprocal suppressive combination of AMP and TET (b, fixed dosage of TET, 20 μg ml^{-1}), AMP and CLI (c, fixed dosage of CLI, 10 μg ml^{-1}) and AMP and FUS (d, fixed dosage of FUS, 20 μg ml^{-1}). **e–h, Reproducibility of the microplating assay between two biological replicates. e,f**, Correlation between the colony forming units (CFU per ml) of two replicates measured during the pairwise drug combination screens (e, Extended Data Fig. 5; f, Extended Data Fig. 4). **g–h**, Correlation between the colony forming units of the two replicates of the multidrug screens (g, left panel, Fig. 2a; g, right panel, Extended Data Fig. 7a; h, Extended Data Fig. 7c). Single, two-drug treatments and high-order drug combinations were differentially coloured as red, light blue and dark blue, respectively. **i**, **The distribution of the killing delays across all single-drug and two-drug treatments**. After taking the best fit of the killing curves to the killing equation (see the killing equation on the caption of Extended Data Fig. 4) we plot the distribution of delay (L) across all conditions. **j–m**, **Nutrient depletion is negligible during the killing assay. j–k**, The optical density (OD, j) and the green fluorescence signal (GFP, k) of the sensitive strain following 8-hour incubation with increasing concentration of cefoxitin. After incubation the supernatant of each well was transferred to a new microplate and was re-inoculated with 2×10^5 GFP tagged cefoxitin resistant strain (MRSA) and incubated for another 6-hour. **l–m**, The OD (h) and GFP signal (i) of the cefoxitin resistant culture after 6-hour incubation.

nature research

Corresponding author(s): Roy Kishony

Last updated by author(s): 2022.07.18

Reporting Summary

Nature Research wishes to improve the reproducibility of the work that we publish. This form provides structure for consistency and transparency in reporting. For further information on Nature Research policies, see our Editorial Policies and the Editorial Policy Checklist.

Statistics

For all statistical analyses, confirm that the following items are present in the figure legend, table legend, main text, or Methods section.

n/a	Confirmed	
☐	☒	The exact sample size (*n*) for each experimental group/condition, given as a discrete number and unit of measurement
☐	☒	A statement on whether measurements were taken from distinct samples or whether the same sample was measured repeatedly
☐	☒	The statistical test(s) used AND whether they are one- or two-sided *Only common tests should be described solely by name; describe more complex techniques in the Methods section.*
☒	☐	A description of all covariates tested
☒	☐	A description of any assumptions or corrections, such as tests of normality and adjustment for multiple comparisons
☐	☒	A full description of the statistical parameters including central tendency (e.g. means) or other basic estimates (e.g. regression coefficient) AND variation (e.g. standard deviation) or associated estimates of uncertainty (e.g. confidence intervals)
☐	☒	For null hypothesis testing, the test statistic (e.g. *F*, *t*, *r*) with confidence intervals, effect sizes, degrees of freedom and *P* value noted *Give P values as exact values whenever suitable.*
☒	☐	For Bayesian analysis, information on the choice of priors and Markov chain Monte Carlo settings
☒	☐	For hierarchical and complex designs, identification of the appropriate level for tests and full reporting of outcomes
☐	☒	Estimates of effect sizes (e.g. Cohen's *d*, Pearson's *r*), indicating how they were calculated

Our web collection on statistics for biologists contains articles on many of the points above.

Software and code

Policy information about availability of computer code

Data collection	The optical density were read by Biotek Synergy 2 plate reader, software version Gene5 1.115. The agar plates were imaged for GFP (excitation:470/30; emission: 540/50) and RFP (excitation: 590/30; emission 641/75) with a custom-made automated imaging device (macroscope).
Data analysis	Code availability statement is provided as a separate section after the data availability statement. The custom python script developed for image analysis is deposited in a public DOI-minting repository (Open Science Framework) and was cited in the appropriate Methods section. The detailed algorithm for calculating the drug interaction scores is available in the Methods section.

For manuscripts utilizing custom algorithms or software that are central to the research but not yet described in published literature, software must be made available to editors and reviewers. We strongly encourage code deposition in a community repository (e.g. GitHub). See the Nature Research guidelines for submitting code & software for further information.

Data

Policy information about availability of data

All manuscripts must include a data availability statement. This statement should provide the following information, where applicable:

- Accession codes, unique identifiers, or web links for publicly available datasets
- A list of figures that have associated raw data
- A description of any restrictions on data availability

The raw data including all the micro-plating images with the bacterial colonies that support the findings of this study are available as Source Data files in a public DOI minting repository (https://osf.io/ypbj5/).

Field-specific reporting

Please select the one below that is the best fit for your research. If you are not sure, read the appropriate sections before making your selection.

☒ Life sciences ☐ Behavioural & social sciences ☐ Ecological, evolutionary & environmental sciences

For a reference copy of the document with all sections, see nature.com/documents/nr-reporting-summary-flat.pdf

Life sciences study design

All studies must disclose on these points even when the disclosure is negative.

Sample size	We screened the cell viability of 2 biologically independent strains (DsRed, GFP) measured in 585 drug conditions (28 singles(1X, 2X dose; at 6 and 4 independent experiments) and 91 pairs at 2 independent experiments; 5x 36 singles (1X,2X,3X,4X,5X and 6X dose), 5x57 multidrug mixes) at 2 independent experiments; 1-5 timepoints; 2-time ranges (short and long-term killing) and 4 to 8 plating (dilutions+technical replicates). The sample size was chosen to allow detection of possible outliers while still allowing a vast systematic quantification of pairwise and multi-drug interactions. Sample size for the larvae experiments was large enough to allow statistically significant detection of variation assuming the Mann Whitney test. Growth inhibition interactions between all the pairwise combinations of the 14 antibiotics were measured as the final optical density of the cultures under a 2-D concentration gradients (8x12 different concentrations). Then a a polynomial surface model (Loess-fit, degree 2) was fitted to the normalized optical density values.
Data exclusions	At the last time point of the early-killing and the long-term clearance assay , 15µL aliquots from each well of the assay plates were also inoculated into a 96-well plate with 150µL liquid LB containing, in each well, the same antibiotic concentrations of the assay plates and incubated overnight at 37°C, 250rpm. Following incubation, OD was measured and growing cultures (OD600>0.2), indicating the presence of resistant cells, were excluded from further analysis. We excluded these wells to specifically focus on the survival fraction of the sensitive cell population. Micro-plating spots where the colonies merged extensively or with too dense colonies to reliably count were designated "uncountable" (over 100 colonies per spot).
Replication	Our high-throughput cell viability assay was highly reproducible, showing good agreement among the independent experiments (Extended Data Fig. 12a-d). The number of biologically independent replicates and experiments for each experiments are listed in the appropriate figure legends.
Randomization	The allocation of the single and multi drug conditions were randomized on the 96-well plates during the high-throughput screen to measure early and long-term killing interactions.
Blinding	The surviving colonies were counted in the presence of different compounds in the same way, while blind to the compound identity of each well.

Reporting for specific materials, systems and methods

We require information from authors about some types of materials, experimental systems and methods used in many studies. Here, indicate whether each material, system or method listed is relevant to your study. If you are not sure if a list item applies to your research, read the appropriate section before selecting a response.

Materials & experimental systems

n/a	Involved in the study
☒	☐ Antibodies
☒	☐ Eukaryotic cell lines
☒	☐ Palaeontology and archaeology
☐	☒ Animals and other organisms
☒	☐ Human research participants
☒	☐ Clinical data
☒	☐ Dual use research of concern

Methods

n/a	Involved in the study
☒	☐ ChIP-seq
☒	☐ Flow cytometry
☒	☐ MRI-based neuroimaging

Animals and other organisms

Policy information about studies involving animals; ARRIVE guidelines recommended for reporting animal research

Laboratory animals	Larvae of the Galleria Mellonella at their final instar stage were used to assess the clearance efficacy of drug combinations. Larvae were either purchased from UK BioSystem Technology (TrueLarv) or from Israel Agricultural Research Organization, Volcani Institute (AROLarv).
Wild animals	*Provide details on animals observed in or captured in the field; report species, sex and age where possible. Describe how animals were caught and transported and what happened to captive animals after the study (if killed, explain why and describe method; if released, say where and when) OR state that the study did not involve wild animals.*

Field-collected samples	*For laboratory work with field-collected samples, describe all relevant parameters such as housing, maintenance, temperature, photoperiod and end-of-experiment protocol OR state that the study did not involve samples collected from the field.*
Ethics oversight	Ethical approval is not required.

Note that full information on the approval of the study protocol must also be provided in the manuscript.